Available online at www.sciencedirect.com
ScienceDirect
Journal of Sound and Vibration 322 (2009) 581–611
JOURNAL OF SOUND AND VIBRATION
www.elsevier.com/locate/jsvi

Experimental unfolding of the nonlinear dynamics of a cable-mass suspended system around a divergence-Hopf bifurcation

Giuseppe Rega[a], Rocco Alaggio[b,*]

[a]Dipartimento di Ingegneria Strutturale e Geotecnica, Sapienza Università di Roma, 00197 Roma, Italy
[b]Dipartimento di Ingegneria delle Strutture, Acque e Terreno, Università dell'Aquila, 67040 Monteluco di Roio, (L'Aquila), Italy

Received 17 May 2008; received in revised form 12 January 2009; accepted 26 January 2009
The peer review of this article was organised by the Guest Editor

Abstract

Systematic experimental investigation of the finite amplitude dynamics of a multiple internally resonant suspended cable-mass, subjected to anti-phase support motion at primary resonance, is accomplished. Upon getting hints from a basic system configuration assumed as reference setup about the multiple bifurcation event possibly governing transition to complex dynamics, an improved experimental apparatus is used to make it technically accessible. Results obtained by varying three control parameters, namely the frequency and amplitude of excitation and the temperature of a thermostatic chamber embedding the experimental system, allow us to characterize in-depth various occurring classes of motion in terms of time and spatial complexity, to describe peculiar and/or persistent features of transition to nonregular dynamics, and to trace them back to a canonical scenario from bifurcation theory. Variable response paths are detected via bifurcation diagrams and spectra of singular values of measurement results, and overall behaviour charts are built in the excitation parameter space. Considering the temperature as a controllable parameter shows to be fundamental for: (i) indirectly setting cable material properties to values for which the conjectured codimension 2 bifurcation becomes apparent, (ii) qualitatively referring the experimental unfolding of regular and nonregular cable dynamics to the theoretical unfolding of the divergence-Hopf bifurcation normal form, and (iii) determining system response not only in the strict neighbourhood of the organizing divergence-Hopf bifurcation but also in the ensuing postcritical regions where the dependence of material damping on temperature affects secondary bifurcations to low-dimensional homoclinic chaos.

1. Background and motivation

Finite amplitude dynamics of suspended cables have been addressed in the last two decades by referring to variably refined theoretical models, through purely analytical, numerical or mixed treatments [1–4]. Yet, there is a need for understanding the actual nonlinear behaviour of suspended cables also through physical models, which are important both for validating theoretical predictions and for detecting new or complex phenomena

*Corresponding author.
E-mail address: ala@ing.univaq.it (R. Alaggio).

0022-460X/$ - see front matter © 2009 Elsevier Ltd. All rights reserved.
doi:10.1016/j.jsv.2009.01.060

Nomenclature

Bifurcations

d-H	divergence-Hopf bifurcation
he	homoclinic explosion
H	Hopf bifurcation
pd	period doubling bifurcation
pf	pitchfork bifurcation
pl	phase locking
sc	saddle connection
scy	saddle cycle
sn	saddle-node bifurcation

Cable-mass suspension modes

H1	first symmetric out-of-plane (horizontal) mode
H2	first antisymmetric out-of-plane (horizontal) mode
V1	first symmetric in-plane (vertical) mode
V2	first antisymmetric in-plane (vertical) mode

Decomposition of the flow

p_i	signal power percentage associated with the ith POM
POM	proper orthogonal mode
Σ	total signal power

Identified motion classes

CHMk	chaotic response
PmMk	periodic motions
QPmMk	quasiperiodic motions on two torus with m attractor periodicity and k number of involved POMs, generally coinciding with the dimension of the invariant manifold M where the motion develops
(R)	resonant
(S)	symmetric
(SC)	symmetric couple

Parameters

f	support motion amplitude, peak-peak voltage of input signal to the shaker amplifier
T	temperature (°C)
v	frequency (Hz)
μ	damping

associated with system nonlinearities but often un-modeled in theoretical analyses. This has produced a few experimental investigations on different cable models, however restricted to the analysis of either system response in regular regime [5,6] or of specific response features of nearly taut [7–9] or sagged [10] cables.

In contrast, quite a systematic analysis of experimental nonlinear cable dynamics has been accomplished in a few papers dealing with a hanging cable/mass system subjected to different harmonic motions of the supports and realizing, for relatively low excitation frequencies, a fairly reliable model of the bare suspended cable. By considering various external/internal resonance conditions, interest has been first devoted to analyzing and classifying the local and overall system response—in either a regular or nonregular regime—in a control parameter plane [11,12], and then to characterizing some main features of complex response and bifurcation mechanisms by properly reconstructing the dynamics from experimental measurements [13,14].

A general overview on the richness and robustness of two different—quasiperiodic and homoclinic—bifurcation scenarios to chaos occurring in various regions of control parameter space has been presented in Ref. [14], by referring to various internally resonant cables, kinds of support motion, and external resonances. However, while the quasiperiodic transition to chaos through a tori breakdown has been addressed quite exhaustively and satisfactorily [13], only some preliminary, yet promising, results were obtained as regards the scenario seemingly involving the global bifurcation of a homoclinic invariant set of the flow. Yet, homoclinic bifurcation to low-dimensional chaos involving just two main—though variable—proper orthogonal modes (POMs) shows to be quite a robust scenario with respect to variations of both cable geometrical-mechanical parameters and excitation conditions [14], thus being a scenario of *general* interest.

Thus, focusing on the homoclinic bifurcation of a multiple internally resonant cable under anti-phase support motion at primary resonance, the present work aims at going in-depth into the experimental characterization of this transition scenario, by analysing the relevant peculiar and/or persistent bifurcation

features and by possibly tracing them back to a canonical scenario from dynamical systems theory. More specifically, the interest is in: (i) performing a systematic physical investigation aimed at characterizing in detail the most robust response features, (ii) possibly frameworking the experimental results within a reference theoretical scenario, and (iii) understanding phenomena responsible for the onset of experimental nonregular dynamics in the relevant background.

From a theoretical viewpoint, homoclinic (and heteroclinic) orbits are known to play an important role in the mechanisms responsible of transition to chaos in multi-degree-of-freedom (d.o.f.) dissipative dynamic systems [15,16], and the relevant framework [17,18] can indeed furnish a valuable interpretative support to the experimental investigation. It is worth reminding one that homoclinic orbits, which are trajectories bi-asymptotic to a saddle limit set, provide a recurrent mechanism for global folding of the phase space, whereas the saddle set furnish the local stretching, folding and contraction representing the necessary prerequisites for the eventual onset of homoclinic chaos.

Within this general context, we aim at verifying the hypothesis that a preliminarily observed scenario of transition to chaos could be explained by experimentally localizing and characterizing a divergence-Hopf (d-H) codimension 2 bifurcation point in control parameter space, and by investigating the local unfolding of the system dynamics.

As a matter of fact, ''multiple bifurcations hold the key to the understanding of the origin of complicated behaviours in dynamical systems'' [19], with the secondary and higher order bifurcations occurring in the relevant neighbourhood often leading to complex dynamics. Typically, in dynamical systems theory, it has been found that nonlinear phenomena predicted by local bifurcation studies also persist for parameter values substantially far from those required for degeneracy [19], so that, provided the relevant 'organizing centre' is localized, the local unfolding of the dynamics can often explain the system behaviour not only locally.

Local bifurcations are classified according to the stability eigenvalues crossing the imaginary axis, and their codimension is the difference between the dimension of the parameter space and the dimension of the corresponding bifurcation boundary or, equivalently, the number of constraints (i.e., independent conditions) imposed on the control parameters to attain the critical point (Ref. [16], see also Ref. [15]). A codimension 2 bifurcation like the d-H is characterized by a double instability where a stationary instability (vanishing of a real eigenvalue) interacts with an oscillatory one (vanishing of the real part of a complex conjugate couple of eigenvalues) producing a critical point $(0, \pm i\omega)$ and one associated eigenspace of marginal stability of dimension three.

Such a codimension 2 local bifurcation can produce all of the invariant sets needed to give rise to homoclinic chaos when, by varying a control parameter, the periodic invariant set approaches the saddle one up to becoming homoclinic to it.

In view of identifying the canonical bifurcation scenario which is likely to be lurking in the background of experimental cable results, some symmetries—though imperfect—exhibited by the physical system and by its response are also of main importance. Overall, it has been stated that systems possessing symmetries generically undergo multiple bifurcations [20]. In particular, in the unfolding of d-H bifurcation the existence of homoclinic bifurcation has been established [21].

All of the previous issues claim for accomplishing a systematic investigation of the suspended cable transition scenario, aimed at: (i) qualitatively and quantitatively characterizing the variable, regular and nonregular, classes of system motion in various control parameters ranges in terms of time and spatial complexity and (ii) detecting the conjectured occurrence of the d-H bifurcation point which is likely to trigger the homoclinic bifurcation to chaos.

The work is organized as follows. In Section 2, upon shortly describing the setup and the techniques adopted in the experimental investigation, the overall response of the reference system in the excitation parameter space is presented, by providing some first hints on the transition from the directly excited single-mode periodic motion up to complex response. The improved, thermally conditioned, experimental system is presented in Section 3, and is then referred to for systematically unfolding the dynamics of the cable-mass suspension system with respect to three varying control parameters, with temperature being added to the excitation amplitude and frequency. This allows us to highlight a strong response sensitivity to temperature variations, while at the same time referring the experimentally observed bifurcation paths to a known canonical scenario from dynamical systems theory. Specifically, the most robust paths and classes of motion in the range of medium temperatures are presented in Section 4, with the unfolding of the experimental *regular*

dynamics around the d-H point being interpreted against a theoretical scenario in Section 5. Sections 6 and 7 are respectively devoted to characterizing the experimental *nonregular* dynamics most reliably identified at low temperature values, and to referring them to a coherent known scenario of transition to chaos. The paper ends with some conclusions and a few perspectives about parallel on-going theoretical developments.

2. Response regimes and transition to chaos in the reference experimental system

When dealing with continuous systems undergoing finite amplitude vibrations, there is a strong possibility of response regimes involving several spatial modes in regular or nonregular nonlinear behaviour. Reliable and complete descriptions of many possible regimes in control parameter space are of main importance. Rich and varied response charts exhibiting regions of different classes of motion are usually obtained, depending on also the realization of meaningful external/internal resonance conditions. Quasiperiodic and chaotic motions are often seen to occur mostly in between regions of clearly dominating low-dimensional regular responses. Accordingly, one major effort is devoted to investigating possible *finite dimensionality* in the complex dynamics of infinite-dimensional systems, and to detecting *minimum numbers* and features of *configuration variables* actually needed to describe complex motions.

As far as the cable is concerned, an experimental model of an elastic cable with concentrated masses hanging from two supports undergoing vertical, harmonic, anti-phase motion is considered (Fig. 1). System mechanical and geometrical properties realize a condition of 2:2:1 internal resonance amongst the frequencies of the first antisymmetric in-plane (vertical, V2) mode, the first antisymmetric out-of-plane (horizontal, H2) mode, and the first symmetric out-of-plane (horizontal, H1) mode. No-contact devices (optical cameras) are used to measure the two (in-plane and out-of-plane) components of motion of four masses at variable locations along the cable.

Previous isolated results allow one to conjecture that a scenario involving the global bifurcation of an homoclinic invariant set could be responsible for transition to chaos when the system is excited at primary resonance of the first antisymmetric in-plane mode (V2) [14]. Experimental observations furnish some evidence of the onset of such an homoclinic invariant set when the forcing frequency reaches the upper bound of the stability region—in the excitation parameter space—of a two-component quasiperiodic response involving shapes which resemble quite well the V2 and H2 modes of the model. An overview of the observed classes of motion is given in Table 1. Dimensionality is characterized in terms of both time and spatial complexity. *Time complexity* is evaluated by calculating invariant measures of the dynamics through the delay embedding procedure [22–25]. Besides Poincaré map inspection and power spectra analysis, information about the dimension of the quasiperiodic and chaotic attractors is obtained from correlation dimension evaluations [26] carried out on time-delay reconstructed phase spaces. In turn, *spatial complexity* is tackled via two approaches: (i) by relating the embedding dimension of the reconstructed attractors to the dimension of the linear phase space, which gives information on the involved number of d.o.f., and (ii) by analysing the spatial

(a)

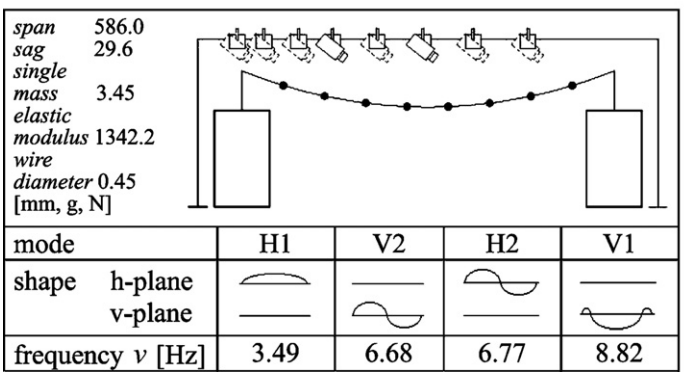

(b)

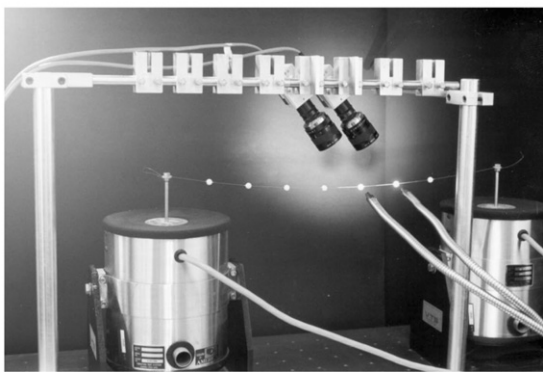

Fig. 1. (a) Mechanical model with system parameters and dynamic characteristics and (b) experimental setup.

Table 1
An overview of motion class characterization.

Attractor		Dimension						Modes
		D_C	D_S	D_E	D–T	No. POMs	D_P	
Periodic	P1M1	1	2	1–3	1	1	3	V2
	P1M2	1	2	1–3	2^R	2	5	V2H2
Quasiperiodic	QP1M2	2	4	2–5	2	2	5	V2H2
	QP2M3	2	4	2–5	3^R	3	7	V2H1H2
Chaotic	CHM2	2.39	4	3–7		2 (94.2%)	5	V2H2
	CHM3	3.18	6	4–9		3 (96.8%)	7	V2H1H2

D_C is the attractor estimated correlation dimension, D_S is the embedding dimension corresponding to dimension invariant saturation, D_E is the expected embedding dimension variation range according to the relationship $[D_C] \leqslant D_E \leqslant (2[D_C]+1)$, where [ ] means the nearest greater integer (the upper bound limit is given by the Mané theorem), D–T column shows the dimension of possibly resonant (R) invariant tori if it exists, No. POMs column shows the number of experimental eigenfunctions identified and the relevant signal power percentage if less than 98%, D_P is the dimension of phase–space required to display the main system dynamics, last column lists the natural cable-mass modes to whom the experimental eigenfunctions can be referred.

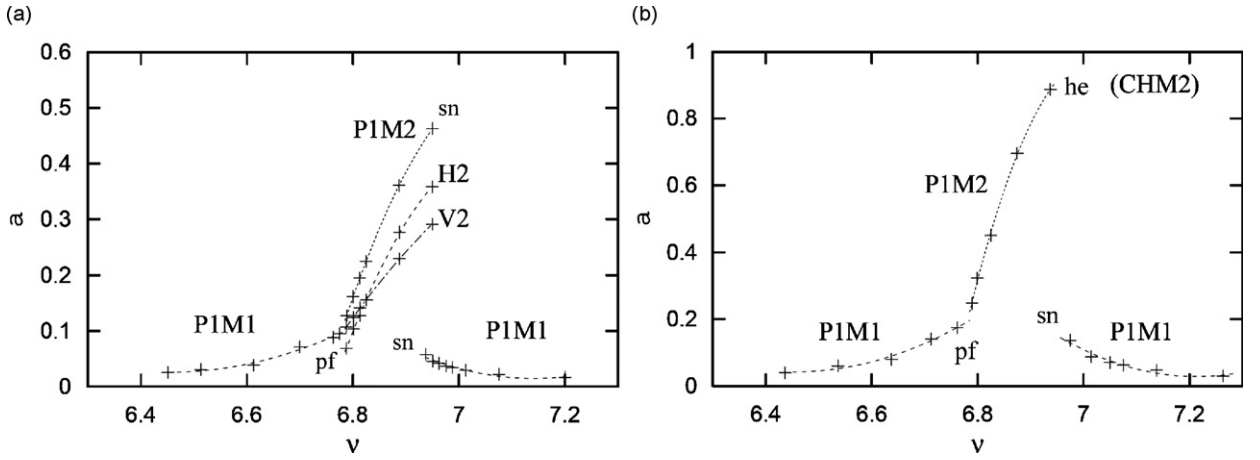

Fig. 2. Frequency-response curves for low forcing levels: (a) $f = 200$ mV and (b) $f = 700$ mV.

structure of the nonregular flow through the proper orthogonal decomposition [27], which allows the identification of the dominant experimental eigenfunctions corresponding, from the mechanical viewpoint, to the configurations most visited, on average, during the system spatio-temporal evolution.

Classification of motions is made based on topological dimension of manifolds where they develop (growing, in regular regime, from one to three-torus) and on correlation dimension of attractors (from one to three in regular regime, coinciding with their local topological dimension; non-integer in chaotic regime). Regular motions are labeled PmMk, periodic, QPmMk quasiperiodic on two torus, with the labels giving information on the attractor periodicity (m) and on the number of involved POMs (k), the latter coinciding with the dimension of the invariant manifold where the motion develops unless the manifold is resonant $^{(R)}$.

Yet, major efforts in experimental analyses actually consist of properly characterizing: (i) the reference bifurcation paths leading to complex attractors, (ii) the extent of regions of complex response, and (iii) the robustness of transition mechanisms in parameter space. A reference bifurcation path for the considered cable ensues from the frequency-response diagram of Fig. 2a, which is obtained for growing excitation frequency ν and a quite low value ($f = 200$ mV) of support motion amplitude measured by the peak-peak voltage of the input signal to the shaker amplifier. The resonant one-mode periodic solution P1M1, involving the directly excited V2 mode, bifurcates through a pitchfork (pf) bifurcation towards a two-mode periodic solution P1M2. Actually, two two-mode solutions coexist corresponding to clockwise and counter-clockwise 'balloonings'

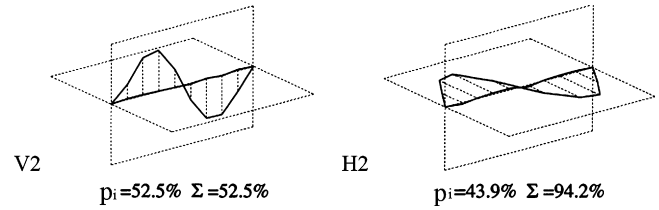

Fig. 3. First two POMs evaluated inside the lower dimension chaotic region.

contributed by both the (in-plane) V2 mode and the driven (out-of-plane) H2 mode—involved in a nearly 1:1 internal resonance—with different phase shifts. The branches of the two contributing components are also reported in Fig. 2a, whereas the corresponding dominant POMs are shown in Fig. 3, with p_i, Σ being the signal power percentage associated with the ith POM and total one, respectively. Both two-mode solutions become unstable due to a saddle-node (sn) bifurcation, where the response jumps down onto the nonresonant branch of the one-mode periodic solution P1M1. Sweeping the frequency down highlights a classical superposition region between one-mode and two-mode solutions.

When increasing the excitation amplitude, the system starts exhibiting transition to chaos. The frequency-response curve in Fig. 2b, corresponding to 700 mV, shows that, at a critical frequency value, each of the two coexisting two-mode solutions loses stability—via a seemingly homoclinic explosion (he)—toward nonregular response, whose existence region ends up with a jump down onto the one-mode solution.

An overall experimental behaviour chart is depicted in Fig. 3 in the frequency-amplitude excitation plane. The motion class labels reported in the various zones refer to Table 1, with the bottom horizontal lines corresponding to the two considered values of excitation amplitude.

For amplitudes higher than 700 mV, the two-mode (P1M2) solution established through the pf loses stability toward a quasiperiodic response QP1M2 (eventually undergoing a torus-doubling), and finally ends up with a non-regular response. The post-critical behaviour is very rich even in the regular regime, where other-though less robust—dynamic phenomena are observed, including phase locking, high periodicity response and two-mode solution period-doublings PmM2 ($m = 5,10,\ldots$).

For even higher excitation amplitudes (above 4 V), in a wide frequency range the response is affected by cable loosening, which makes characterization of the overall dynamics quite difficult (as reflected by less specific labels in Fig. 4) and non-systematic. Yet, qualitative observation suggest that for amplitudes higher than about 6 V and growing frequency, the P1M1 directly forced response loses stability due to a Hopf (H) bifurcation instead of a pf one, and is then followed by transition to nonregular dynamics.

Accordingly, the following *conjecture* can be made based on investigation of the reference system: at amplitude and frequency values close to 6 V and 6.4 Hz, respectively, two Hopf and pf bifurcation loci coalesce in a codimension 2 bifurcation point which is able to organise the overall dynamics and transition to chaos.

However, in the experimental investigation, the possibility of getting reliable and systematic observations at high excitation amplitudes is strongly limited by the too high values of amplitudes involved in the response, which also entail cable loosening. A further main problem occurs in the overall investigation. Given the long transients sometimes needed by the very flexible system to attain steady responses, robust characterization of its dynamics is sometimes very time demanding and fairly questionable, also in connection with the ambient temperature changes occurring during experimental observations. As a matter of fact, such changes are likely to meaningfully affect the cable material properties, thus having important effects on the possibility of reliably characterising the bifurcation paths we are interested in.

3. The thermally conditioned experimental system

To tackle the issues mentioned above, improvements are accomplished in both the experimental setup and the system response investigation.

A modified apparatus is obtained by embedding the mechanical system in a thermostatic chamber designed to finely set the temperature at a constant value. A feedback control system sets the current flow in a Peltier cell array and keeps the temperature constant inside the insulated chamber wherein the cable and four optical

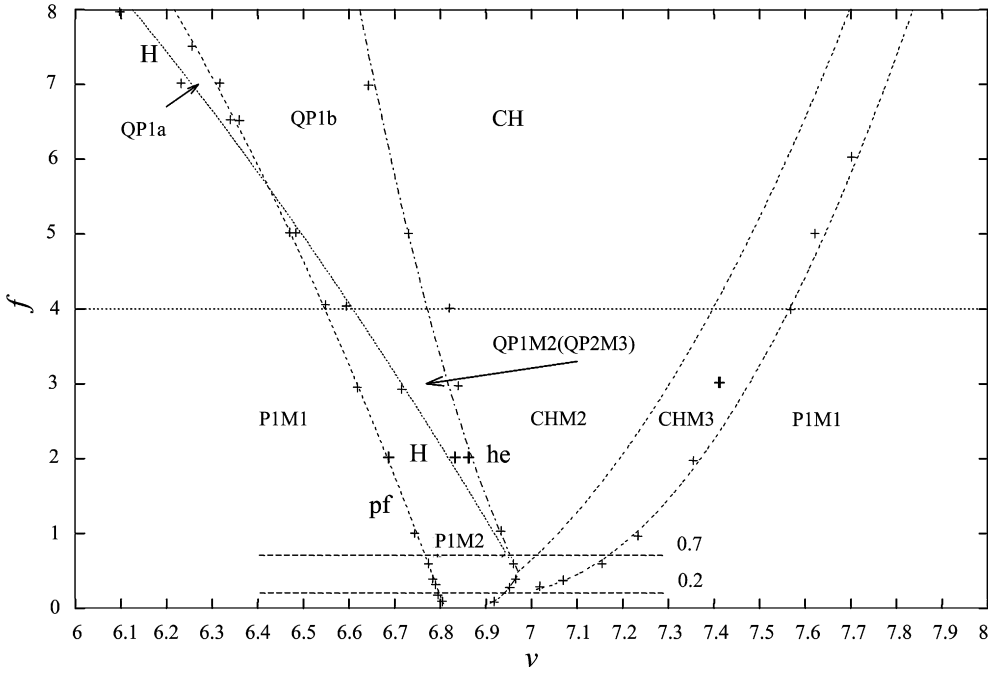

Fig. 4. Experimental behaviour chart (in the frequency (Hz) vs amplitude (V) plane of support motion).

cameras targeting sub-miniature LEDs glued to the masses are contained. Overall, thermally conditioning the system stabilizes its response, thus making the previously time consuming systematic analysis feasible and reliable.

In addition, the thermally controllable setup allows us to improve the mechanical accessibility to the range of higher excitation amplitudes which turn out to be of major interest for a systematic characterization of the transition scenario possibly ensuing from the conjectured d-H bifurcation event. The underlying idea is to indirectly modify the linear and nonlinear dissipation of the system by changing the chamber temperature. As a matter of fact, considering the temperature as a further independently controllable parameter, besides the excitation amplitude and frequency, may allow us to get a richer unfolding of the experimental dynamics, by also possibly affecting some secondary bifurcations which, based on the reference system results, are likely to be responsible for the homoclinic-like chaotic response observed in the post-critical frequency region. This further enlarges the target of a systematic investigation to be conducted under different, thermally controlled, conditions. In particular, from a physical viewpoint it may be expected that globally lowering system linear dissipation within the controlled apparatus is substantially equivalent to increasing the excitation nominal amplitude towards the range of higher values where the conjectured d-H bifurcation may be robustly accessed and reliably identified. Such an expectation is theoretically confirmed by a companion on-going analysis [28,29]. Within this perspective, the linear dissipation of the experimental system can be globally lowered by indirectly affecting the cable material damping via changing the chamber temperature. The loss factor of viscoelastic materials is strongly temperature (and frequency) dependent and the relevant laws change with the material; so, a characterization of the system linear damping vs temperature is first performed showing how, in the considered temperature range, damping decreases with decreasing temperature.

Fig. 5 reports the values of some main modal parameters (frequency ν (Hz) (a) and damping μ (percent) (c)), as well as some relevant ratios (b, d), as obtained for different values of chamber temperature T (°C), with the identification being performed after stabilization of the parameters. It is worth noticing how the ratios between couples of frequencies involved in the 2:2:1 resonance condition do not change with temperature (Fig. 5b), the mean ratio between anti-symmetric in-plane or out-of-plane frequency and symmetric out-of-plane frequency being 1.96 or 1.98, respectively, with a very small standard deviation (<0.4 percent). In contrast, the effect of temperature is evident both on single modal dampings (Fig. 5c), where it entails changes

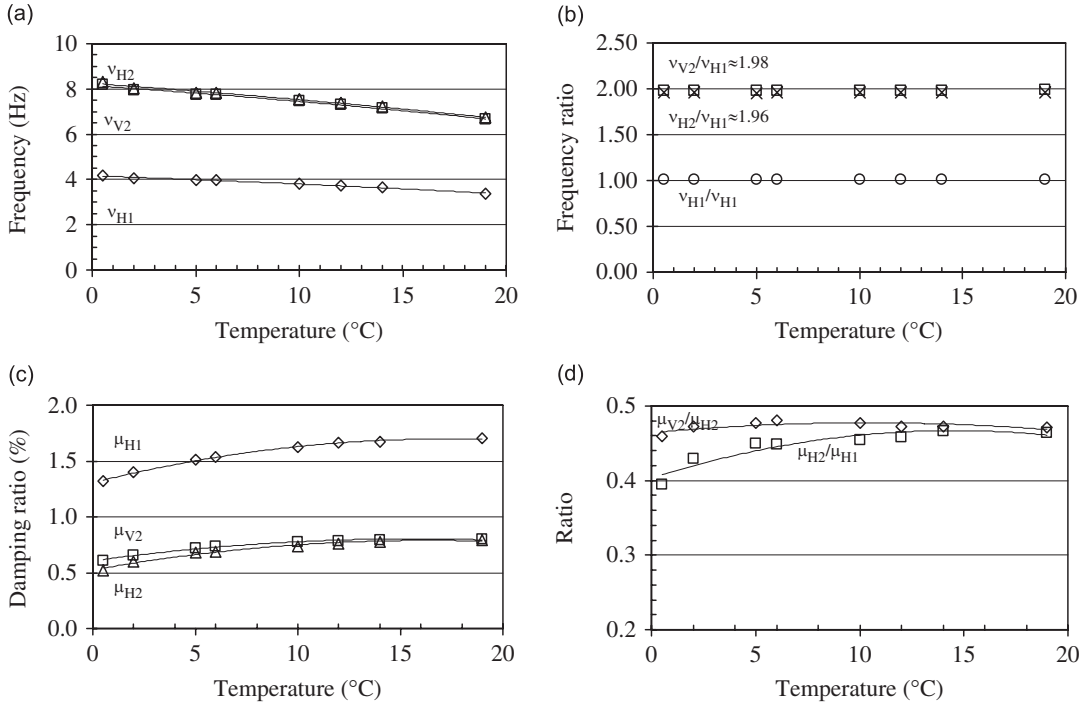

Fig. 5. The effect of temperature: (a) on modal frequencies, (b) on the ratio between modal frequencies, (c) on modal dampings, and (d) on their ratios.

up to 52 percent (μ_{H2}) with respect to a reference temperature ($T = 0.5\,^{\circ}C$), and, to a lower extent, on the ratio between modal dampings (Fig. 5d), which changes up to 18 percent (μ_{H2}/μ_{H1}).

In the following, a quite systematic analysis of the experimental response as obtained at various chamber temperatures, ranging from the reference one (ambient temperature $T = 19$–$21\,^{\circ}C$) considered in Section 2 up to rather low values ($T \approx 0\,^{\circ}C$), will be reported, by summarizing the meaningfully different behaviours observed in various sub-ranges. The same experimental and numerical techniques as those mentioned in Section 2 are used for detecting time and space dimensionality of the system response, along with the same terminology and labelling for the identification of the various observed classes of motion in terms of dynamic (periodic, quasiperiodic, chaotic), topological (manifolds where they develop), and mechanical (main contributing spatial shapes) features.

4. Regular regimes and transition to chaos scenario at medium temperature values

4.1. Chamber temperature 12 °C

Results are summarized in the behaviour chart and the companion table of Fig. 6, with the (a)–(d) labels in the latter referring to alternative bifurcation paths followed when sweeping the excitation frequency up ($\rightarrow$) or down ($\leftarrow$). The excitation frequency in the chart is also adimensionalized with respect to the natural frequency of the first in-plane antisymmetric mode, whereas the amplitude of the support motion is measured by the peak-peak voltage. Bifurcation diagrams and spectra of singular values of the covariance matrix of measurement results for various values of excitation amplitude and growing frequency are also reported (Figs. 7, 8, 10, and 11).

The former show the response amplitude a in the one dimensional projection of the Poincaré section of the configuration space, whereas the latter, along with the companion experimental eigenvectors, gives information about the response dimensionality obtained by linearly decomposing the covariance matrix of the spatial flow, each singular value measuring the percentage p of signal power associated with the respective

(a)

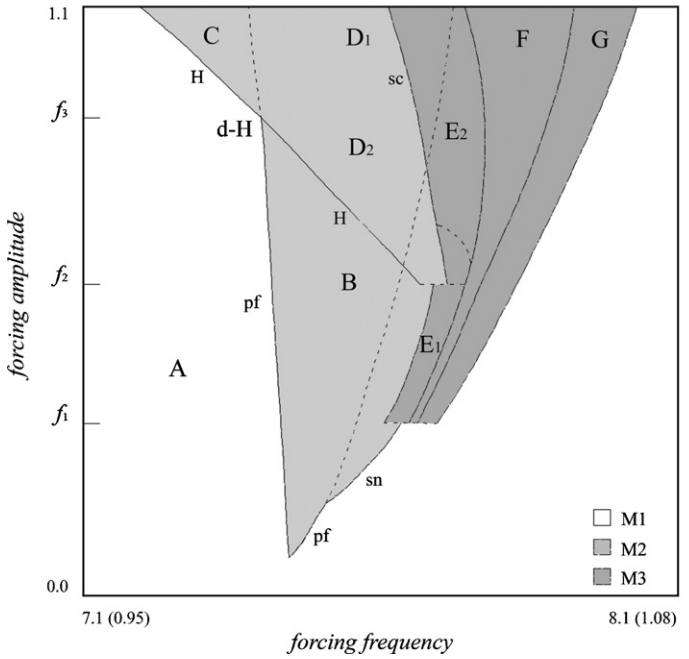

(b)

Zone		Attractor	Dimension			Modes
			Dc	D-T	POMs	
A		P1M1	1	1	1	V_2
C		QP1M1	2	2	1	V_2
B		$P1M2^{(SC)}$	1	2^R	2	V_2H_2
D1		$QP2M2^{(S)}$	2	2	2	V_2H_2
		$QP2M2^{(SC)}$	2	2	2	V_2H_2
D2		$QP1M2^{(SC)}$	2	2	2	V_2H_2
E1	(a)	QP1M3	2	3^R	3	$V_2H_2H_1$
	(b)	QP2M3	2	3^R	3	$V_2H_2H_1$
	←	P1M1	1	1	1	V_2
E2	(a)	QP1M3	2	3^R	3	$V_2H_2H_1$
	(c)	P2M3	1	3^R	3	$V_2H_2H_1$
←→	(d)	P1M1	1	1	1	V_2
F	(a)	CHM3	2.8		3	$V_2H_2H_1$
	(b)	P2M3	1	3^R	3	$V_2H_2H_1$
	←	P1M1	1	1	1	V_2
G	(b)	P2M3	1	3^R	3	$V_2H_2H_1$
		P1M1	1	1	1	V_2

Fig. 6. $T = 12\,^{\circ}C$: (a) qualitative behaviour chart (frequencies in Hz and adimensionalized with respect to $v_{V2} = 7.5$ Hz, forcing amplitude in V) and (b) characterization of motion classes.

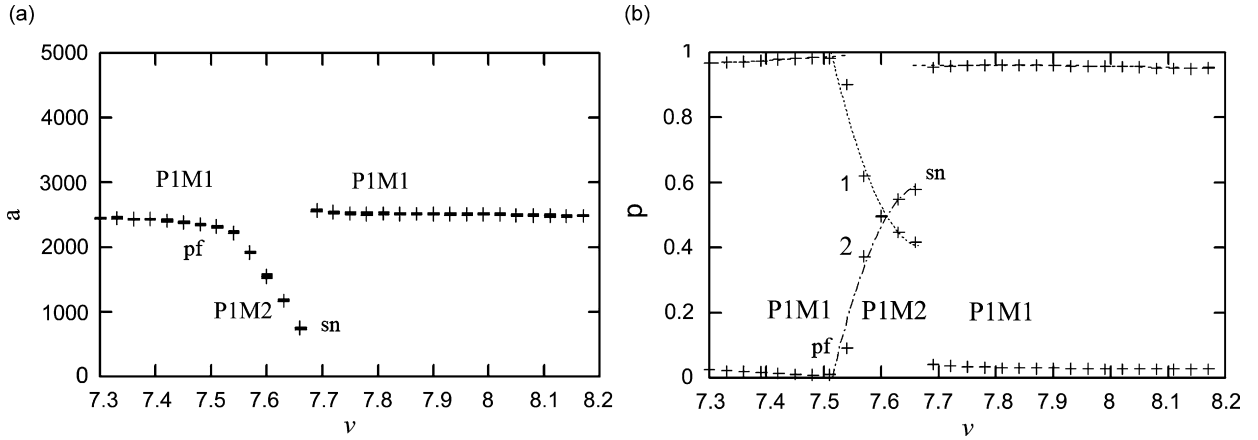

Fig. 7. Bifurcation diagram (a) and singular value spectrum (b): antisymmetric in-plane (1) and out-of-plane (2) POMs.

experimental eigenvectors in the flow decomposition [27]. It is worth noticing that these singular values spectra can be regarded as response curves reporting separately the power percentage of each experimental eigenfunction.

Overall, the structure of the behaviour chart confirms the organizing role played by the codimension 2 bifurcation event suggested by the analysis of the reference system. However, the description of the many occurring, and often competing (depending on initial conditions), classes of motion is herein much more detailed for being the relevant outcomes definitely more robust in time. Rich and complex responses do occur within the wide range wherein the directly forced one-mode solution P1M1 is unstable. Bifurcation paths and stability diagrams are discussed in the sequel by distinguishing among four ranges of increasing excitation amplitude.

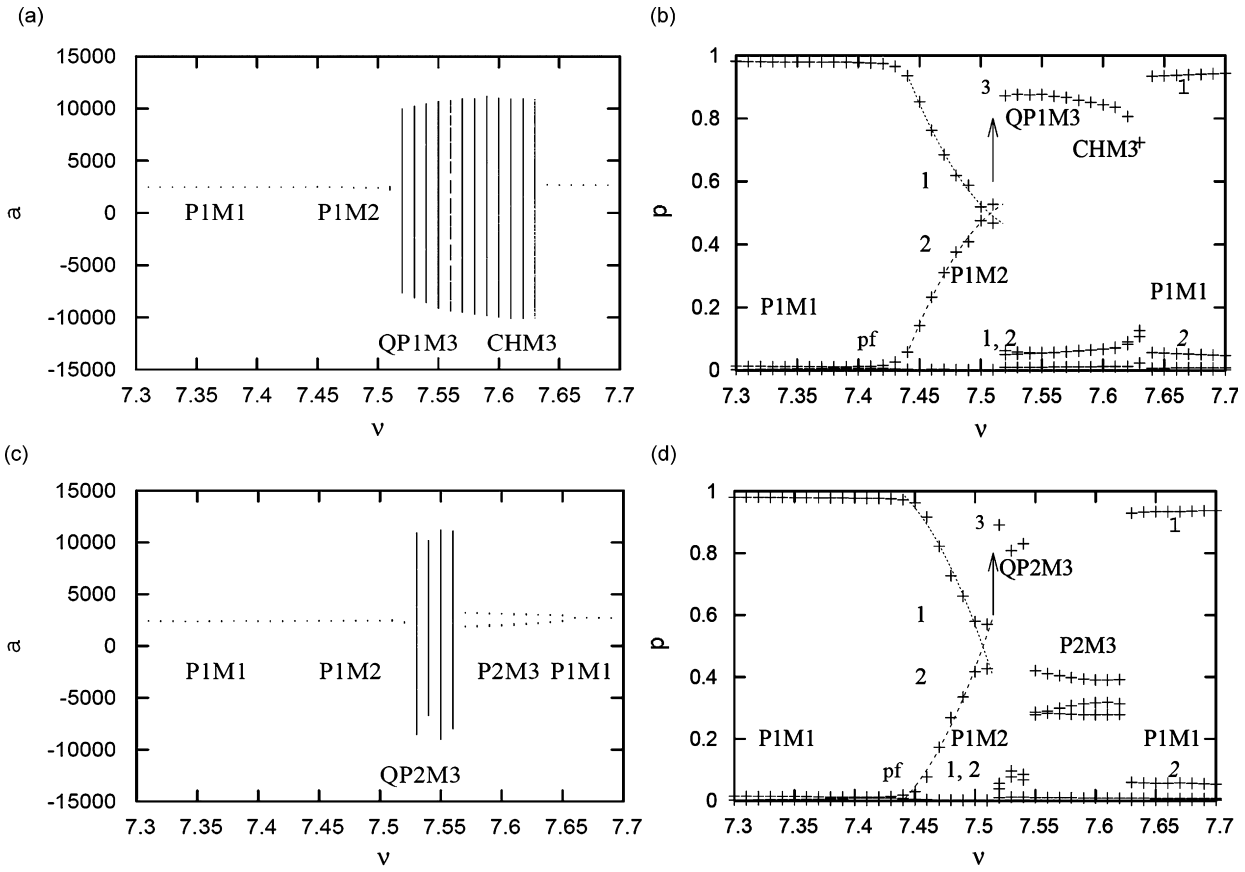

Fig. 8. Motion classes: P1M1, P1M2; in (a,b) QP1M3, CHM3; in (c,d) QP2M3, P2M3.

(i) *Excitation amplitude* $f<f_1$: For amplitudes lower than f_1 (see Figs. 6 and 7), the P1M1 solution bifurcates to a two-mode periodic response (P1M2) with increasing frequency. A symmetric couple $P1M2^{(SC)}$ of competing two-mode ballooning responses occurs owing to system symmetry. In the following, reference will be arbitrarily made to either one of the two elements of the couple, unless being necessary to distinguish between them. The experimental eigenvector (POM) involved in the P1M1 response (labelled 1 in Fig. 7b) clearly resembles the first antisymmetric in-plane mode of the cable-mass suspension, whereas the POM labelled 2 closely resembles the first antisymmetric out-of-plane mode (i.e., the two modes observed in the reference system, see Fig. 2), the singular value of the latter bifurcating from zero at the pf producing the two-mode $P1M2^{(SC)}$ response (Fig. 7b). A jump brings the response back to P1M1 for growing frequency.

(ii) *Excitation amplitude* $f_1<f<f_2$: In this range, the scenario becomes more involved (Fig. 8). At the end of the stability region (B label in Fig. 6) of $P1M2^{(SC)}$, the dynamics alternatively settle onto two competing subcases: (a) QP1M3 quasiperiodic response evolving, with increasing frequency, toward nonregular CHM3; (b) QP2M3 quasiperiodic response, stable in a thin range and ending in periodic P2M3. The M3 label highlights a meaningful involvement in the response of a third recognizable component (labelled 3 in Fig. 8b and d):

$$\mathrm{P1M1} \rightarrow \mathrm{P1M2}^{(\mathrm{SC})} \rightarrow \left\{ \begin{array}{ll} \text{(a)} & \mathrm{QP1M3} \rightarrow \mathrm{CHM3} \rightarrow \mathrm{P1M1} \\ \text{(b)} & \mathrm{QP2M3} \rightarrow \mathrm{P2M3} \rightarrow \mathrm{P1M1} \end{array} \right\}$$

Subcases (a) and (b) are alternatively accessed for the same parameters after an abrupt bifurcation marked anyway by the intervention of a POM resembling the first symmetric out-of-plane mode (M2→M3). In subcase (a), which is the most robust at higher excitation amplitudes: (i) the involvement of a symmetric shape in quasiperiodic motion does not produce torus doubling, QP1M3 being needed for the evolution towards the otherwise unreachable nonregular response CHM3, and (ii) motion classes QP1M3 and CHM3 established upon

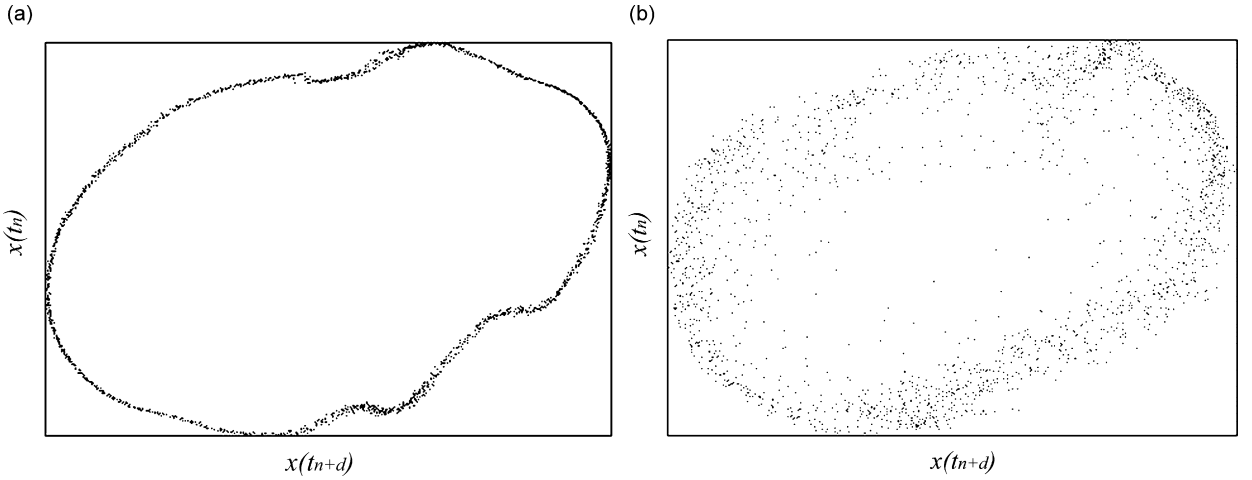

Fig. 9. Time delay reconstruction. Projection of Poincaré section on $x(t_n), x(t_{n+d})$ plane: (a) QP1M3 and (b) CHM3.

an unclear bifurcation mechanism mainly involve the out-of-plane symmetric shape and evolve on nearby manifolds (Fig. 9). In subcase (b), which is relatively more robust for lower amplitudes: (i) QP2M3 is a torus doubled quasiperiodic response involving the symmetric out-of-plane component in $\frac{1}{2}$ subharmonic regime (due to the existing 2:1 internal resonance) and (ii) the same three shapes do decompose the flows associated with both QP2M3 and P2M3, though with different relative importance.

(iii) *Excitation amplitude* $f_2<f<f_3$: In the higher f_2–f_3 range (Fig. 10), the transition from P1M2 to chaos reveals the occurrence of a Hopf bifurcation preceding the involvement of the third component in QP1M3 motion. The overall path (see also the table in Fig. 6) is as follows:

$$\mathrm{P1M1} \underset{\mathrm{pf}}{\longrightarrow} \mathrm{P1M2^{(SC)}} \underset{\mathrm{H}}{\longrightarrow} \mathrm{QP1M2^{(SC)}} \rightarrow \left\{ \begin{array}{ll} \text{(a)} & \mathrm{QP1M3} \rightarrow \mathrm{CHM3} \rightarrow \mathrm{P1M1} \\ \text{(b)} & \mathrm{QP2M3} \rightarrow \mathrm{P2M3} \rightarrow \mathrm{P1M1} \\ \text{(c)} & \mathrm{P2M3} \rightarrow \mathrm{P1M1} \\ \text{(d)} & \mathrm{P1M1} \end{array} \right\}$$

In particular:

- $\mathrm{P1M2^{(SC)}}$ bifurcates through Hopf toward a quasiperiodic (clockwise/anti-clockwise) symmetric couple $\mathrm{QP1M2^{(SC)}}$ on the same two-dimensional sub-manifold already embedding the periodic response; the two associated spatial shapes (labels 1 and 2 in Fig. 10b, d and f) still resemble quite closely the first in-plane and out-of-plane antisymmetric modes of the cable-mass suspension, respectively.
- $\mathrm{QP1M2^{(SC)}}$ bifurcates alternatively for the same control parameter towards four competing subcases: (a) and (b) as in the lower amplitude range, plus (c) and (d); all ensuing responses, except P1M1, involve the first symmetric out-of-plane mode.
- For sweeping down frequency, $\mathrm{QP1M2^{(SC)}}$ directly bounds the P1M1 region.

In all (a)–(d) subcases the transition mechanism from $\mathrm{QP1M2^{(SC)}}$ is unclear and produces a very long transient with M3 ending to quite different solutions, far away from the imposed continuity initial condition. This long transient response is likely to mark a global bifurcation involving also a third dimension (label 3, corresponding to H1 mode, in Fig. 10) with non-negligible signal power. The clearer situation occurs in subcase (d), whose $\mathrm{QP1M2^{(SC)}} \rightarrow \mathrm{P1M1}$ bifurcation causing simultaneous disappearance of two two-dimensional symmetric invariants of the flow is conjectured to be a global structurally unstable saddle connection. Yet, the same kind of global bifurcation is possibly responsible also for the $\mathrm{QP1M2^{(SC)}}$ instability giving rise to the other competing responses. A more apparent characterization of the bifurcations bounding the $\mathrm{QP1M2^{(SC)}}$ response will be obtained at lower temperatures.

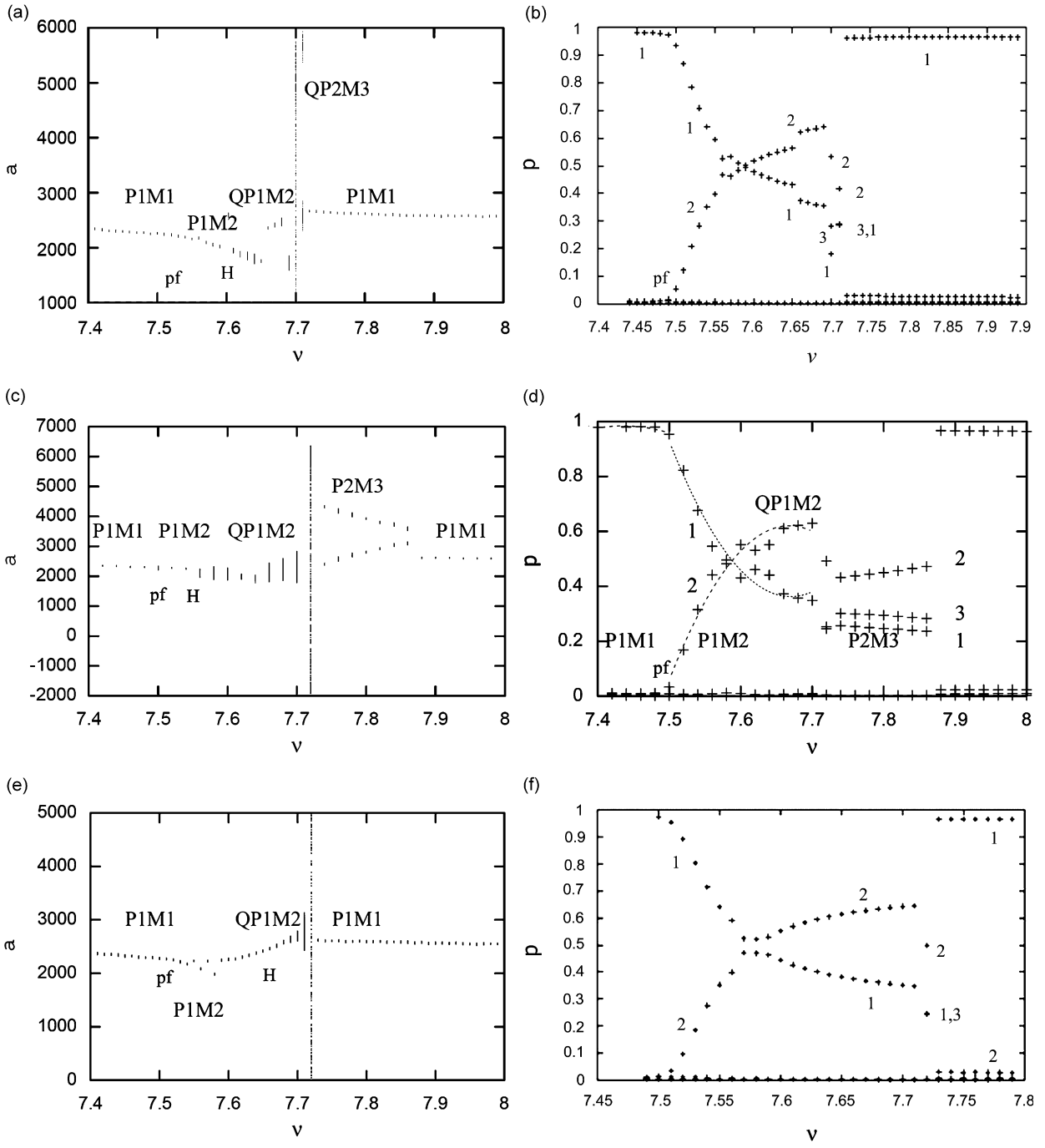

Fig. 10. Subcases b (a,b), c (c,d), and d (e,f).

It is worth noticing that, unlike the f_1–f_2 amplitude range, bifurcations towards QP2M3 and then P2M3 responses (subcase (b)) are rare and confined to lower forcing in the f_2–f_3 range.

(iv) *Excitation amplitude* $f>f_3$: As expected based on qualitative hints from a companion analytical model [28,29], lowering the temperature allows us to reach a critical excitation amplitude corresponding to the d-H bifurcation which was conjectured to exist on the resonant branch of the P1M1 solution. In fact, for excitation amplitudes higher than the critical value f_3, the Hopf bifurcation precedes the divergence.

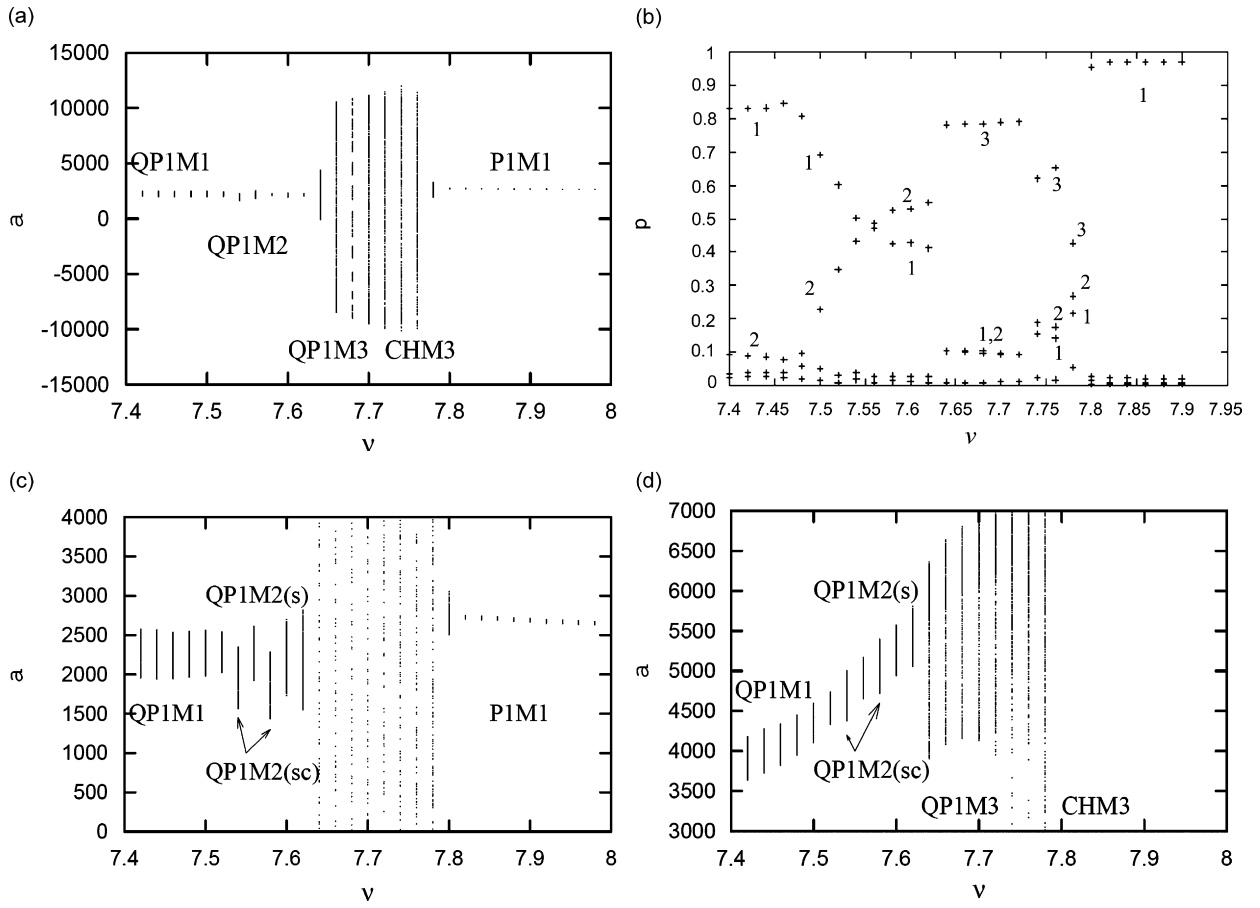

Fig. 11. Subcase a. In (c,d), horizontal and vertical projections of Poincaré sections, respectively, with two realizations of QP1M2$^{(SC)}$ occurring at 7.52 and 7.56 Hz.

In Fig. 11 results relevant to an amplitude above the critical point are reported ($f = 1.05$ V). The one-mode solution P1M1 bifurcates to QP1M1 due to Hopf. In turn, this evolves towards a QP1M2$^{(S)}$ (with $^{(S)}$ standing for symmetric, see also the table in Fig. 6) two-mode quasiperiodic response (label 2) as the frequency exceeds a critical value marked by the abrupt growth of percentage participation of shape 2 to the flow decomposition (Fig. 11b).

For growing frequency, QP1M2$^{(S)}$ bifurcates alternatively towards QP1M3 or P1M1:

$$\mathrm{P1M1} \underset{\mathrm{H}}{\longrightarrow} \mathrm{QP1M1} \underset{\mathrm{pf}}{\longrightarrow} \mathrm{QP1M2}^{(\mathrm{S})} \rightarrow \left\{ \begin{array}{ll} \text{(a)} & \mathrm{QP1M3} \rightarrow \mathrm{CHM3} \rightarrow \mathrm{P1M1} \\ \text{(d)} & \mathrm{P1M1} \end{array} \right\}$$

However, it is important to notice that, herein, the most robust symmetric QP1M2$^{(S)}$ competes on M2 with the already observed QP1M2$^{(SC)}$ symmetric couple: enlargements of Poincaré section projections in bifurcation diagrams show two sections relevant to QP1M2$^{(SC)}$, intertwined with the most robust QP1M2$^{(S)}$ (the former being distinguishable from the latter only if projecting the flow onto a proper plane).

As frequency increases, QP1M3 motion (involving also a third dimension, label 3) and finally CHM3 nonregular response are evidenced. It is worth noticing that the transition to nonregular dynamics involves QP1M3 on the whole investigated amplitude range.

If the frequency is swept down, a wide superposition range between the lower (nonresonant) branch of the one-mode response P1M1 (see Fig. 2) and various post-critical responses is observed on the right part of the behaviour chart, with the stability range of the former bounding the QP1M2 range.

Further lowering the temperature will allow to focus on the characterization of the dynamics in the neighbourhood of codimension 2 bifurcation point.

4.2. Chamber temperature 6 °C

Overall, lowering the temperature entails: (i) lowering the critical forcing amplitude corresponding to codimension 2 bifurcation and (ii) shifting the range of involvement of out-of-plane symmetric mode towards lower frequencies, thereby producing, in general, higher dimensional responses at lower frequencies in regular dynamics while at the same time allowing to highlight, for higher frequencies, an interesting path to nonregular dynamics on a low-dimension manifold (M2). This results in a clearer scenario both in the regular regime—where no period doubled classes of motion P2M3, QP2M3 exist—and in the transition to the CHM3 nonregular one, which directly settles upon the global bifurcation bounding the stability range of $QP1M2^{(SC)}$ with no interposition of other motion classes. In between, transient (or structurally unstable) chaos on M2 (CHM2) develops.

Even if lowering the temperature entails changing the dimension of the linear manifolds embedding regular motion classes, with respect to $T = 12\,^{\circ}\mathrm{C}$, both the topological dimension of the solutions and the bifurcation scenarios unfolding the overall dynamics remain unchanged, showing the existence of an underlying organizing framework not affected by qualitative changes in this temperature range. Being the d-H codimension-2 bifurcation point and the two anti-symmetric eigenfunctions (POMs 1 and 2) identified in the experiments sufficient to unfold a companion theoretical stability diagram (see Sections 5 and 7), motion classes embedded in M2 (or in its sub-manifold M1), as picked up for $T = 12\,^{\circ}\mathrm{C}$, are assumed to be the experimental basic realizations of the scenario. Accordingly, in the following, classes possessing a further dimension (besides that of the POM minimum number, M2 or M1) are denoted by appending an integer prime $(+n)$ to the relevant labels.

The behavior chart (Fig. 12) and the stability diagrams are discussed by distinguishing between amplitude ranges below (Fig. 13) and above (Figs. 14 and 15) the critical value ($f_c = 0.28\,\mathrm{V}$, $v_c = 7.8\,\mathrm{Hz}$) singling out the d-H point.

(i) *Excitation amplitude lower than codimension 2 critical value*: For amplitudes lower than the codimension 2 bifurcation critical value and growing frequency (Fig. 13), the basic response classes are the same as those

(a)

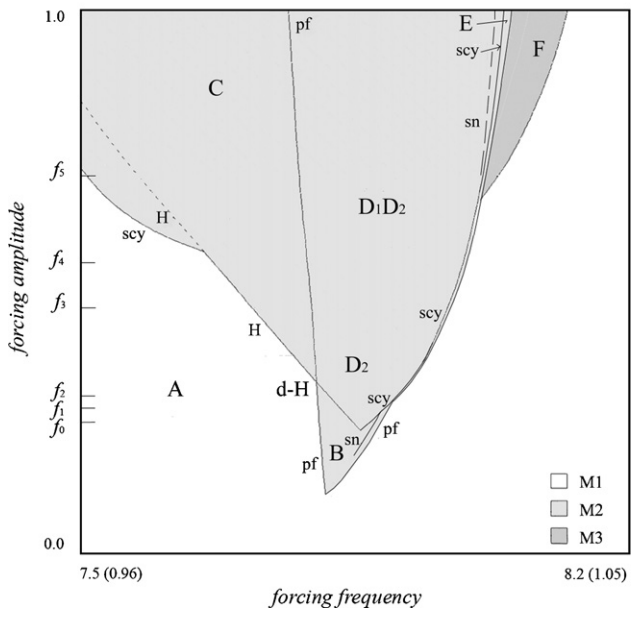

(b)

Zone	Attractor	Dimension			Modes
		Dc	D-T	POMs	
A	P1M1	1	1	1	V_2
C	$QP1M1^{(+1)}$	2	2	1(+1)	$V_2(H_1)$
B	$P1M2^{(SC)}$	1	2^R	2	V_2H_2
D_1	$QP1M2^{(S)}$	2	2	2	V_2H_2
D_2	$QP1M2^{(SC)}$	2	2	2	V_2H_2
E	$CHM2^{(*)}$			2	V_2H_2
F	CHM3	2.7		3	$V_2H_2H_1$
	P1M1	1	1	1	V_2

$^{(*)}$ unstable

Fig. 12. $T = 6\,^{\circ}\mathrm{C}$: (a) qualitative behaviour chart and (b) characterization of motion classes.

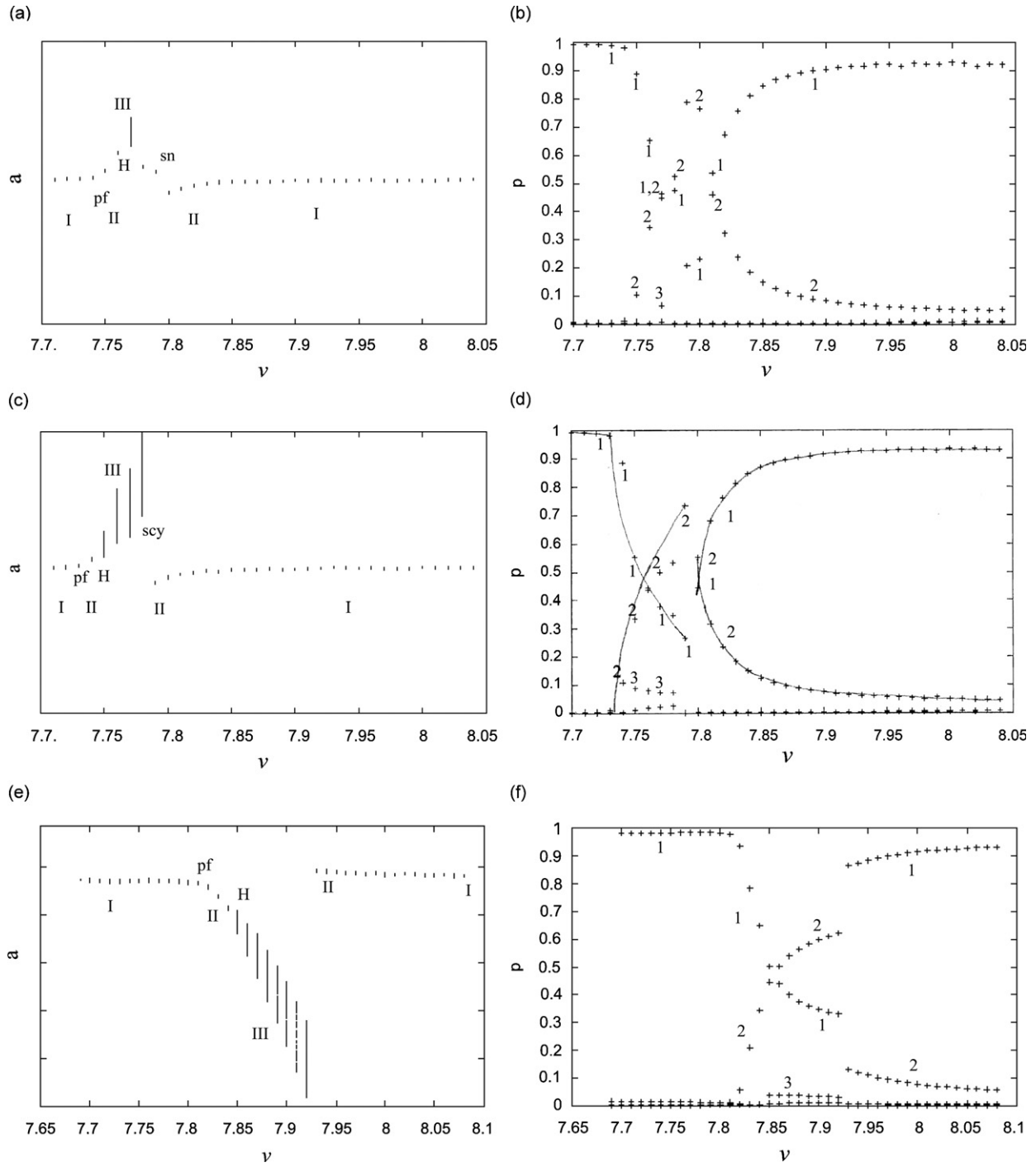

Fig. 13. Subcases f_0, f_1, f_2 in (a,b), (c,d), (e,f), respectively. Motion classes: P1M1 (I), P1M2 (II), QP1M2$^{(SC)}$ (III).

previously described. The solution bifurcates (via pf) from the directly forced P1M1 (label I in Fig. 13a, c and e) to one of the two coexisting symmetric two-mode solutions P1M2$^{(SC)}$ (label II), the latter losing stability through Hopf toward the two quasiperiodic QP1M2$^{(SC)}$ solutions (label III), which in turn bifurcate back to either P1M2$^{(SC)}$ through saddle cycle (scy, subcases f_0 and f_1, in the former case also exhibiting a saddle node) or directly to P1M1 (subcase f_2). Indeed, in the latter case, the formerly unstable

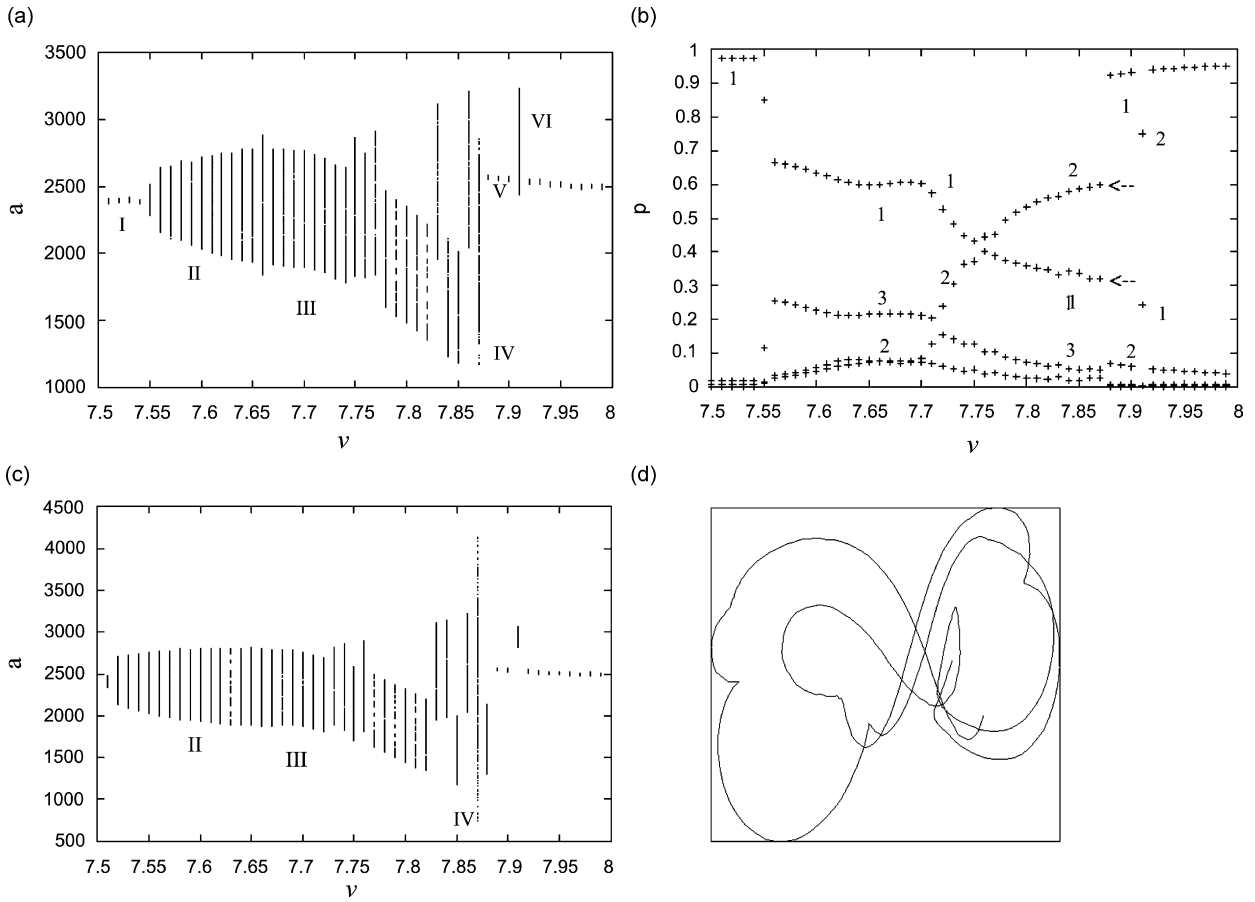

Fig. 14. Subcases f_3, f_4 in (a,b), (c,d), respectively. In (a) P1M1 (I), QP1M1$^{(+1)}$ (II), QP1M2$^{(S)}$ and QP1M2$^{(SC)}$ (III), CHM2 (IV), P1M1 (V). The arrows in (b) mark the flow decomposition relevant to class IV of (a). In the bifurcation diagram (c) at a higher forcing amplitude ($f_4 = 0.48$), the structurally unstable nonregular response on M2 is symmetrically arranged with respect to the cable plane; (d) a two-dimensional projection of a small part of the Poincaré section relevant to class IV of (c) shows a nearly symmetric response in the configuration plane.

fixed point P1M1 is now a stable focus, and the two fixed points corresponding to P1M2$^{(SC)}$ originated at divergence, as well as the limit cycles corresponding to QP1M2$^{(SC)}$, disappear. Fig. 13 shows even clearer bifurcation paths than those reported for higher temperature values.

(ii) *Excitation amplitude higher than codimension 2 critical value*: For amplitudes higher than f_c (Figs. 14 and 15), the Hopf bifurcation precedes the pf. With growing frequency, P1M1 (label I) bifurcates towards a quasiperiodic response (label II) denoted QP1M1$^{(+1)}$, with the integer prime staying for the augmented dimension (due to the increasing involvement of POM 3, symmetric out-of-plane, as the amplitude increases away from d-H bifurcation) with respect to the minimum one of the reference QP1M1 ($T = 12\,^{\circ}$C). Indeed, QP1M1$^{(+1)}$ decomposes mainly on the anti-symmetric shape (POM 1) for lower amplitudes (f_3), whereas for high amplitudes (f_5) (compare Figs. 14b and 15b) the symmetric out-of-plane shape (POM 3) dominates the quasiperiodic response (actually also doubling the attractor periodicity), which also involves the symmetric in-plane shape (POM 4).

The dimensionality analysis in Fig. 14b shows the largely prevailing involvement of anti-symmetric shapes, POM 1 in QP1M1$^{(+1)}$, POMs 1 and 2 in QP1M2$^{(SC)}$. Indeed, with growing frequency, the parameter range is reached where the symmetric couple QP1M2$^{(SC)}$ (label III) is stable, although coexisting with QP1M2$^{(S)}$. Note that the contribution of POM 3 is meaningful in QP1M1 whereas it is much lower in QP1M2$^{(S,SC)}$; accordingly the $^{(+1)}$ superscript is used in the first case while it is skipped in the latter one for the sake of simplicity.

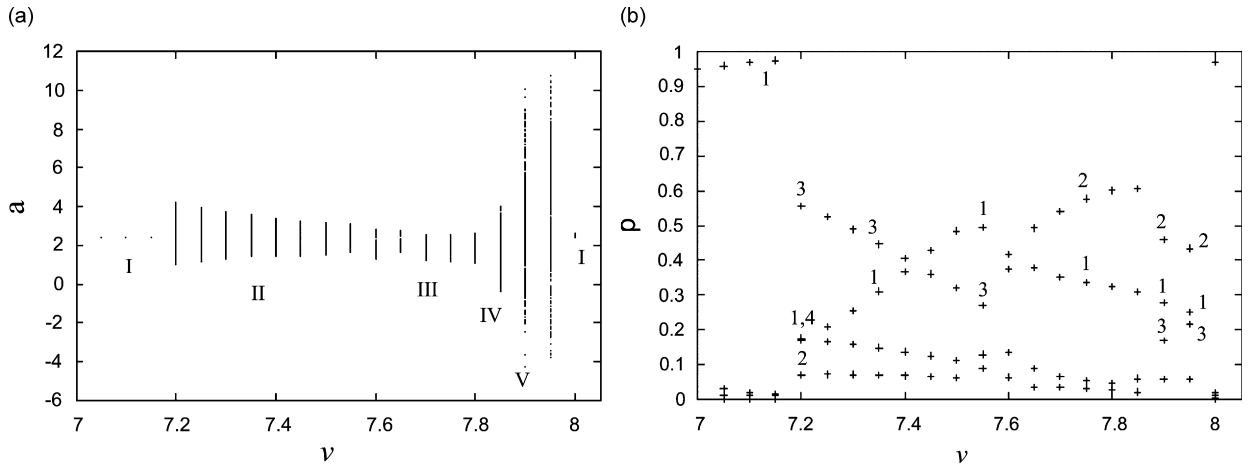

Fig. 15. Subcase f_5 (a much higher amplitude): (a) P1M1(I), QP1M1(II), QP1M2$^{(S)}$, QP1M2$^{(SC)}$(III), structurally unstable nonregular response on M2 (IV), stable CHM3 (V) in a narrow strip on the right boundary and (b) the major contribution of POM 3 in C (QP1M1$^{(+1)}$) and F (CHM3) zones is apparent.

To explain the transition to QP1M2$^{(SC)}$ from QP1M1$^{(+1)}$, a pf bifurcation (affecting one already unstable fixed point) toward QP1M2$^{(S)}$ followed by a global bifurcation (a saddle connection) toward QP1M2$^{(SC)}$ has to be conjectured, consistent with canonical scenarios occurring in the neighbourhood of d-H point (see Section 5). Such a global bifurcation on M2 is supposed to be produced by a tangle between the stable and unstable invariant manifold of the flow responsible for QP1M2$^{(S)}$. Characterization at lower temperature will support this conjecture and will highlight the occurrence of a structurally stable nonregular dynamics of homoclinic type due to an evolution in parameter space of the aforesaid global bifurcation.

Different from the results for $T = 12\,^{\circ}\mathrm{C}$ (see Section 3.1, subcases (iii) and (iv)), herein the nonregular response directly follows the global bifurcation threshold bounding the stability range of QP1M2$^{(SC)}$, with no motion classes involving other experimental eigenfunctions in-between, and it first develops on the M2 manifold (CHM2, label IV in Fig. 14a and c), though being structurally unstable. CHM2 exists in a symmetric couple just like QP1M2 from which it bifurcates (Fig. 14a and b), yet also a symmetric response gluing the two coexisting versions does exist (Fig. 14c and d).

For subcases f_3, f_4 the overall path is as follows:

$$\mathrm{P1M1} \underset{\mathrm{H}}{\longrightarrow} \mathrm{QP1M1}^{(+1)} \underset{\mathrm{pf}}{\longrightarrow} \mathrm{QP1M2}^{(\mathrm{S})} \underset{\mathrm{global}}{\longrightarrow} \mathrm{QP1M2}^{(\mathrm{SC})} \rightarrow (\mathrm{CHM2}^{(\mathrm{S,SC})})_{\mathrm{unstable}} \rightarrow \mathrm{P1M1}$$

even if the existence ranges of QP1M2$^{(S)}$ and QP1M2$^{(SC)}$ do overlap partially.

Increasing the frequency, the structurally unstable nonregular response CHM2 ends in either regular P1M1 (Fig. 14) or stable nonregular CHM3 (Fig. 15) for lower and higher excitation amplitudes, respectively. While CHM2 decomposes on two-dimensional manifold, CHM3 also involves POM 3 (symmetric out-of-plane), though with a low relative percent with respect to the higher temperature where it was dominant.

Summarizing: (i) With respect to lower amplitudes, no main differences occur in the bifurcation path relevant to regular dynamics (however involving a higher number of POMs) and (ii) nonregular response with M2 is transient or structurally unstable: it will become steady (or structurally stable) when further lowering the temperature, which will allow a better unfolding of the motion classes including CHM2 and CHM3 at high excitation amplitudes.

5. Schematic unfolding of regular dynamics around divergence-Hopf bifurcation

Previous bifurcation diagrams have been produced by changing the frequency control parameter while keeping fixed the initial condition at the value attained by the response at previous frequency step. Thus, the obtained behaviour charts do not represent, even in principle, every solution possibly occurring in the

considered parameter range. Other solutions are supposed to be stable and compete with the detected ones, but they would be experimentally accessed only by means of an adequate procedure furnishing the right initial condition at each control parameter step. Nevertheless, the obtained results are sufficient to draw a robust unfolding of *regular dynamics* for the tested cable suspension system; results based on further investigations, reported in Section 6, are instead needed to characterize transition to *nonregular dynamics* (see Section 7).

The obtained information seem to be sufficient to also refer the overall experimental bifurcation scenario to a canonical one in dynamical systems theory. The following main results are of interest in this respect.

(i) The bifurcation scenario is consistent with the unfolding of the dynamics in the proximity of a codimension 2 bifurcation point of divergence-Hopf type. Of course, the theoretical transition scenario ensuing from the unfolding of d-H normal form may have an experimental counterpart provided that in the latter the topological dimension of the observed periodically forced motion classes is reduced by one, i.e. by looking at the experimental Poincaré section (see Section 5.1 in the following).
(ii) Due to the external (anti-phase primary resonance of first anti-symmetric in-plane mode) and internal (1:1 resonance between anti-symmetric in-plane and out-of-plane modes) resonance features, the system dynamics in both the regular and nonregular regime is essentially traceable to participation of two spatial shapes closely resembling the first two anti-symmetric linear modes.

As a matter of fact, a substantial similarity exists between the observed experimental dynamics and the dynamics exhibited in the neighbourhood of a d-H point by theoretical systems. Of course, this can be suitably exploited in the formulation also of a theoretical model of the cable aimed at reproducing the experimental results, and this is the subject of parallel ongoing analyses [28,29]. Herein, we limit ourselves to summarizing the attained information and reorganizing them in the framework of the recognized scenario.

Before doing it, it is worth reminding oneself that two main mechanical parameters, namely the excitation frequency and amplitude, have been considered, respectively, as the primary and secondary control parameters in the experimental investigation; yet, they have been shown to be not the sole ones affecting the system response. In fact, driven by a conjecture about the possibility to unfold the otherwise unreachable dynamics by "externally" varying another secondary parameter, the strong role played also by the temperature in unfolding the experimental dynamics has been highlighted, with many important response features depending on temperature sub-ranges.

In this framework: (i) the obtained results give information to unfold bifurcation scenarios also with respect to temperature; qualitative changes produced by temperature in the bifurcation paths as well as persistent behaviour ranges are recognized, (ii) within the stability range of each persistent path, temperature changes produce quantitative changes in the critical values of the main control parameters (i.e. in the solution's stability margins). This allows one, at some temperature values, to get a better visibility of transition phenomena otherwise obscured by the finite resolution of experimental analysis or by response features inessential to understand the organizing bifurcation mechanism.

Yet, a substantially invariant bifurcation scheme is seen to persist over the whole range of temperature variation, thus allowing us to make a comparison between the reorganized and summarized experimental results and the stability diagrams known to bifurcation theory [15,16]. Indeed, though being the dynamics of the continuous system potentially infinite-dimensional, its unfolding in the neighbourhood of the experimentally highlighted d-H point can be referred to the theoretical unfolding provided by the low-dimensional bifurcation system represented by the d-H normal form [29]. Direct comparison is reasonable provided the manifold embedding the solutions remain the same and bifurcations well resemble bifurcation diagrams of normal form. However, it must be noticed that bifurcation paths of the high-dimensional experimental system may be considerably richer than those of the reference normal forms, for including bifurcations that also involve eigenvalues normal to the invariant planes [30].

5.1. Experimental bifurcation paths (regular dynamics) versus theoretical stability diagram

Experimental bifurcation paths produced in a regular regime for growing frequency with temperature $T \geqslant 6\,^{\circ}\mathrm{C}$ are shortly summarized. Two most robust paths occur in the neighbourhood of d-H point, for forcing

levels respectively higher and lower than the critical value:

$$\text{(i)}\quad \mathrm{P1M1} \underset{\mathrm{H}}{\longrightarrow} \mathrm{QP1M1} \underset{\mathrm{pf}}{\longrightarrow} \mathrm{QP1M2^{(S)}} \underset{\mathrm{global}}{\longrightarrow} \mathit{Q}\mathrm{P1M2^{(SC)}} \rightarrow \mathrm{P1M1}$$

$$\text{(ii)}\quad \mathrm{P1M1} \underset{\mathrm{pf}}{\longrightarrow} \mathrm{P1M2^{(SC)}} \underset{\mathrm{H}}{\longrightarrow} \mathrm{QP1M2^{(SC)}} \rightarrow \mathrm{P1M1}$$

In this temperature range, direct comparison of experimental regular results with a normal form stability diagram is possible provided the experimental path is restricted to parameter regions where none of the (n_s) eigenvalues with negative real part at d-H bifurcation goes beyond the imaginary axis thus producing a bifurcation ending up with the involvement of a new dimension in the response, i.e., in mechanical terms, involving the symmetric out-of-plane mode.

For the sake of comparing the unfolding of experimental results in the neighborhood of d-H point with theoretical scenarios, stability and bifurcation diagrams are sketched in Fig. 16. In this respect it is worth stressing how the stability diagram of the theoretical d-H unfolding consists of a set of autonomous nonlinear equations, possibly in normal form, to be obtained by applying a reduction procedure to an evolution system at the bifurcation boundary and describing the dynamics of the system on a reduced dimension manifold. Instead, in the experimental counterpart, the evolution system is nonautonomous due to the periodic motion of the supports but its Poincaré mapping is autonomous, so that the dynamics of the mapping can be qualitatively compared to the dynamics of the autonomous bifurcation set, provided the physical variables actively involved in the bifurcation are evidenced and distinguished from the non-active variables. Thus, in the comparison, the fixed points of the normal form correspond to those in the Poincaré sections of the experimental results (which represent periodic motion classes of the physical system), with the physical variables involved in the divergence and Hopf being respectively the second and first POM well resembling the first out-of-plane and in-plane antisymmetric linear modes of the cable suspension.

Looking at Fig. 16, experimental solutions and bifurcations can be described as follows, by starting from the region (a) where only the anti-symmetric in-plane POM takes part in the response (focus fixed point P1M1), the solution thus lying on the M1 sub-manifold.

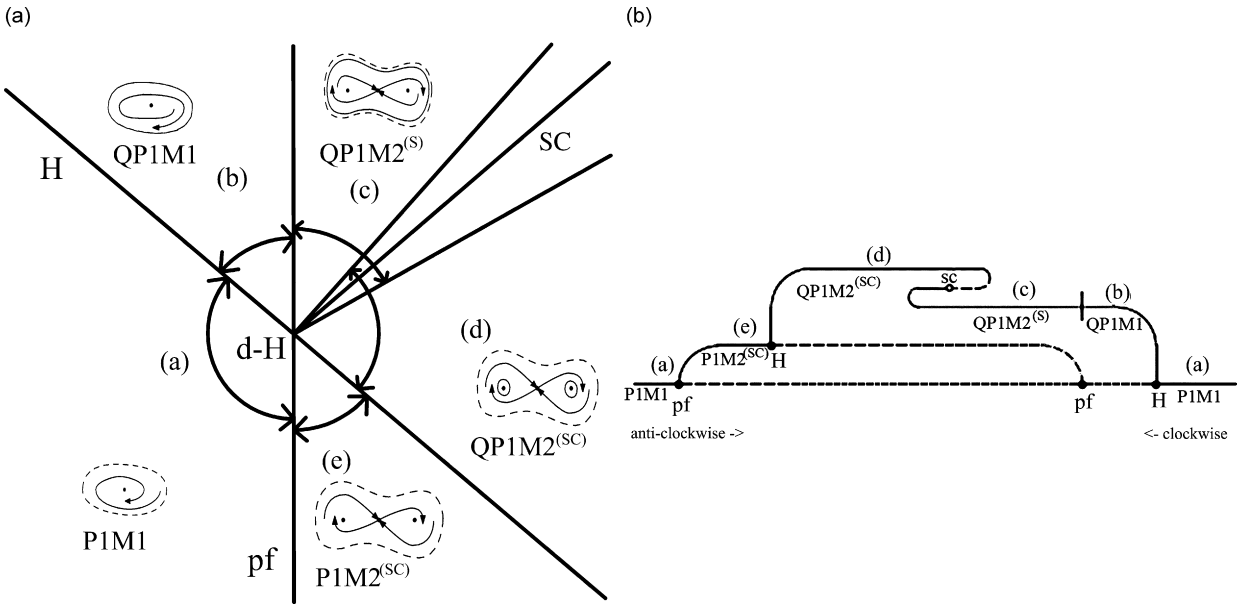

Fig. 16. Schematic (a) stability diagram and (b) experimental bifurcation paths.

Following an anti-clockwise path (corresponding to the former path (ii)) in Fig. 16a:

(i) From (a) to (e), the stable fixed point P1M1 loses stability due to pf to a couple of coexisting symmetric foci P1M2$^{(SC)}$ on a resonant two-torus. At pf, the anti-symmetric out-of-plane experimental eigenfunction (POM 2) enters the response. It is just the involvement of eigenfunction 2 to allow exploiting physical system symmetry to produce symmetric couples; however, due to reflection symmetry, the system has solutions either self-symmetric (prime $^{(S)}$) or being related in symmetric pairs (prime $^{(SC)}$).
(ii) From (e) to (d), the couple of symmetric foci P1M2$^{(SC)}$ bifurcates through Hopf to the couple of limit cycles QP1M2$^{(SC)}$.

Following a clockwise path (corresponding to the former path (i)) in Fig. 16a:

(iii) From (a) to (b), P1M1 fixed point stability is lost through Hopf and a limit cycle (QP1M1) settles, the reference manifold still being M1; in the schematic diagram of Fig. 16b, the unstable fixed point and a stable limit cycle are shown.
(iv) From (b) to (c), a pf bifurcation is trespassed and two new unstable fixed points add to phase space. The pf drives the out-of-plane anti-symmetric eigenfunction (POM 2) into the response, by doubling the manifold dimension (M2). Phase space is characterized by three unstable fixed points and a cross-well limit cycle (QP1M2$^{(S)}$).
(v) From (c) to (d), an homoclinic saddle connection is trespassed corresponding to phase space transition on two-torus from stable cross-well QP1M2$^{(S)6}$ motion to two stable in-well QP1M2$^{(SC)}$ motions.

The represented schematic stability diagram based on experimental bifurcation paths is in full agreement with literature theoretical results [15,16].

However, note that, in both the anticlockwise and the clockwise path, the theoretical unfolding of the phase space transition from QP1M2$^{(SC)}$ stable limit cycles to P1M1 focus fixed point, which occurs in the experimental chart farther away from the d-H point, needs further understanding. Accordingly, this transition is not shown in the two bifurcation paths of Fig. 16b.

6. Regular and nonregular dynamics at low temperature values

While substantially confirming the robust bifurcation framework evidenced in the regular regime at higher temperatures, results relevant to temperatures lower than 6 °C: (i) enrich the patterns of post-critical evolution of response with varying forcing frequency and (ii) disclose clearer, though competing, portraits of transition to nonregular dynamics, which depend on the attained values of low temperature and of forcing amplitude above the d-H point.

6.1. Chamber temperatures 4 and 3 °C

Results relevant to $T = 4\,^{\circ}\mathrm{C}$ are summarized in the behaviour chart of Fig. 17. The main outcomes are: (i) the two coexisting QP1M2$^{(SC)}$ responses (region D) end in nonregular *steady* responses CHM2 on the M2 manifold (region E) also at lower excitation amplitudes and (ii) evidences of *homoclinic* chaos are found in the CHM2 region. About the effect of lowering the temperature on nonregular response regions it can be stated that: (i) the CHM2 motion, already present as transient or structurally unstable chaos at higher temperature, considerably increases its robustness and the extent of its stability range and (ii) the response CHM3 on three-dimensional manifold, formerly dominating the nonregular regime right of the global bifurcation, is shifted to higher excitation frequencies.

The key role played in the transition to nonregular dynamics with M2 by the global bifurcation delimiting the stability range of symmetric solutions QP1M2$^{(SC)}$ becomes clearer (Fig. 18).

The chaotic response region is actually partitioned into two sub-regions: the left one (region E) involves the same contributing POMs already characterizing the quasiperiodic response, i.e. the first in-plane and out-of-plane antisymmetric; the right one (F), accessed from previous sub-region with growing frequency whereas

(a)

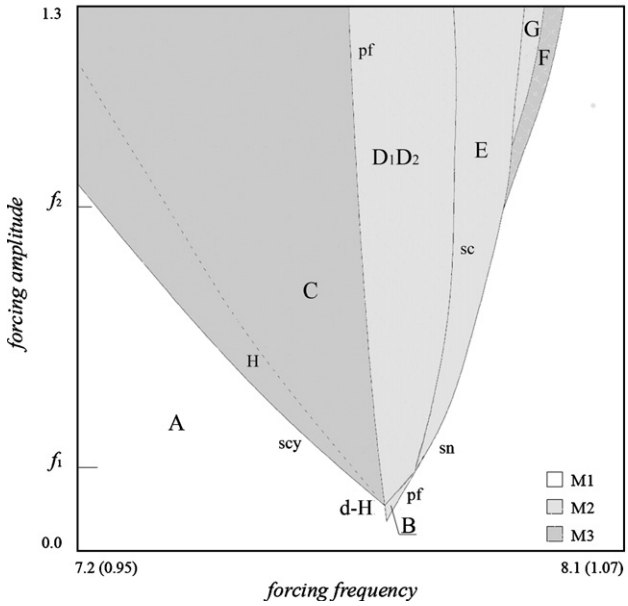

(b)

Zone	Attractor	Dimension			Modes
		Dc	D-T	POMs	
A	P1M1	1	1	1	V_2
B	P1M1	1	2^R	2	V_2
C	$QP1M1^{(+2)(S)}$	2	2	1(+2)	$V_2(H_1V_1)$
D_1	$QP1M2^{(S)}$	2	2	2	V_2H_2
D_2	$QP1M2^{(SC)}$	2	2	2	V_2H_2
E	CHM2	2.3		2	V_2H_2
G	QP5M2	2	2	2	V_2H_2
F	CHM3	3.1		3	$V_2H_2H_1$
	P1M1	1	1	1	V_2

Fig. 17. $T = 4\,^{\circ}C$: (a) qualitative behaviour chart and (b) characterization of motion classes.

inaccessible (Fig. 19) with decreasing frequency, involves also a predominant first symmetric out-of-plane POM (label 3).

In Fig. 19 two bifurcation diagrams (and corresponding singular values spectra) obtained at the same forcing amplitude for increasing and decreasing frequency are reported, respectively. They show the occurrence of small regions of coexistent solutions: e.g., for this excitation amplitude ($f = 1.0$ V), the quasiperiodic solution labelled II coexists with periodic solution P1M1 (label I) in the range 7.16–7.24 Hz, whereas the nonregular response CHM3 (labelled V) coexists with periodic solution P1M1 in the range 7.88–7.94 Hz. Contrary to CHM3, CHM2 (label IV) only occurs in a parameter range where P1M1 is unstable.

The paths for growing and decreasing frequency are, respectively:

$$\mathrm{P1M1} \rightarrow \mathrm{QP1M1^{(+2)}} \rightarrow (\mathrm{QP1M2^{(S,SC)}}) \rightarrow \mathrm{CHM2} \rightarrow \mathrm{CHM3} \rightarrow \mathrm{P1M1}$$

$$\mathrm{P1M1} \leftarrow \mathrm{QP1M1^{(+2)}} \leftarrow (\mathrm{QP1M2^{(S,SC)}}) \leftarrow \mathrm{CHM2} \leftarrow \mathrm{P1M1}$$

In the latter case, P1M1 is bounded by CHM2, while it was bounded by QP1M2 at higher temperatures where stable CHM2 was not found.

Lowering the temperature ($T = 3\,^{\circ}C$), nonregular response on M2 becomes more robust to the detriment of CHM3; bifurcation diagrams in Fig. 20 show the occurrence of an enlarged stability range of CHM2 (label IV) at even lower excitation amplitudes.

For higher forcing amplitudes (Fig. 21), quasiperiodic responses (QP5M2, label V, G region in Fig. 17) are identified in between CHM2 (E) and CHM3 (F) regions:

$$\mathrm{P1M1} \underset{\mathrm{H}}{\longrightarrow} \mathrm{QP1M1^{(+2)}} \underset{\mathrm{pf}}{\longrightarrow} \mathrm{QP1M2^{(S,SC)}} \rightarrow \mathrm{CHM2} \rightarrow \mathrm{QP5M2} \rightarrow \mathrm{CHM3} \rightarrow \mathrm{P1M1}$$

Although in regular dynamics some differences occur between bifurcation diagrams obtained for different temperature values, it is still possible to inscribe them in the framework of d-H normal form stability diagrams, under certain conditions.

(a) Participation of other modes produces motion classes with augmented dimension without entailing qualitative changes with respect to canonical bifurcation diagrams, i.e. topologically equivalent motion

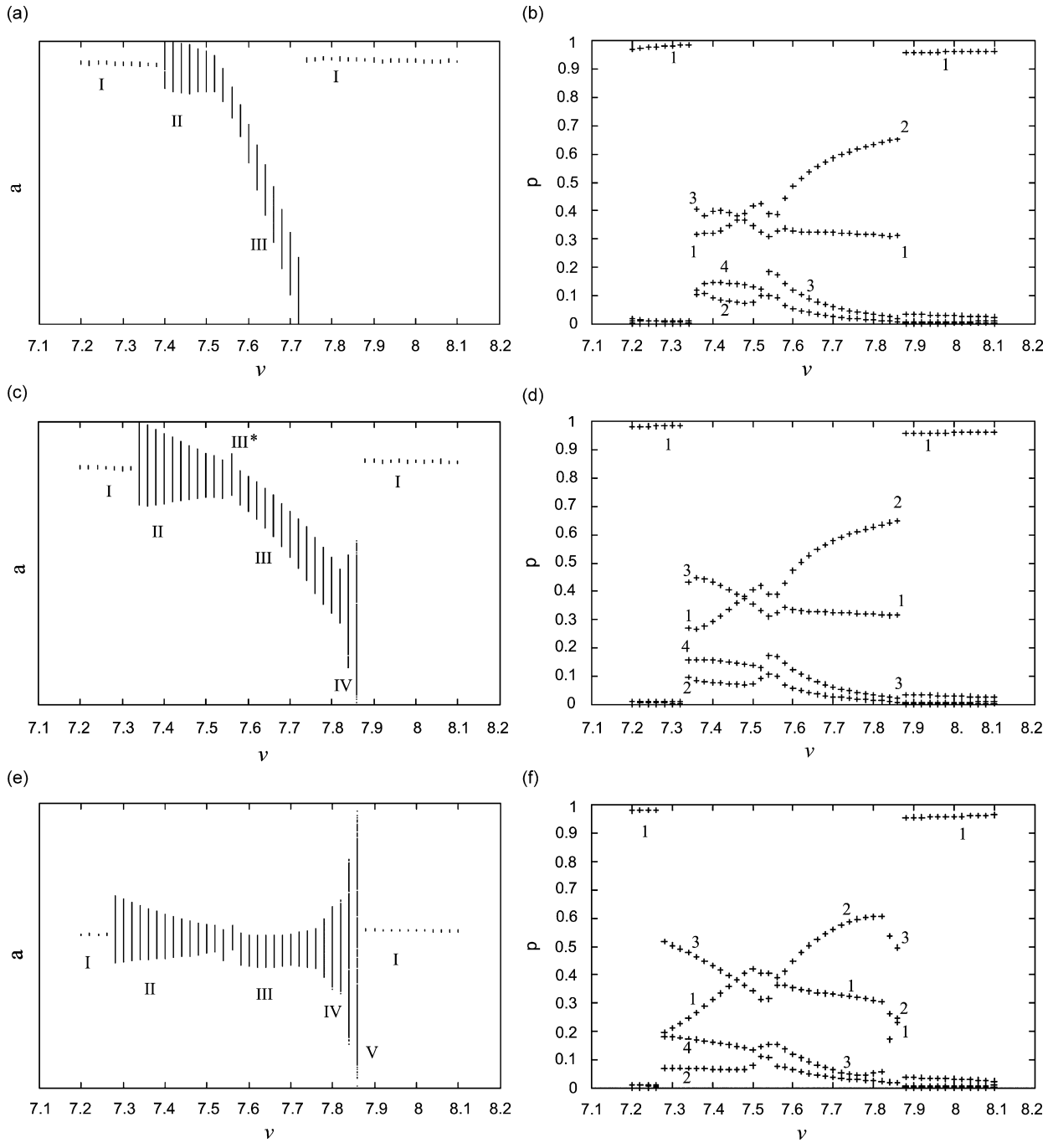

Fig. 18. (a), (b) Forcing amplitude higher than codimension 2 critical value but lower than f_1: the response remains in regular regions; (c), (d) forcing amplitude in between f_1 and f_2: a frequency range of nonregular response (IV) with M2 is reported, bounding QP1M2$^{(SC)}$ on the left (see also QP1M2$^{(S)}$ (III*)) and P1M1 on the right, for growing frequency; (e), (f) higher forcing: a wider range of nonregular response is noticed.

classes bifurcate following the canonical path even if they are embedded in higher order manifolds. From this viewpoint, the bifurcation frame underlying the unfolding of regular dynamics fully complies with the canonical d-H scenario, since it describes dynamics on an invariant manifold whose dimension is reduced

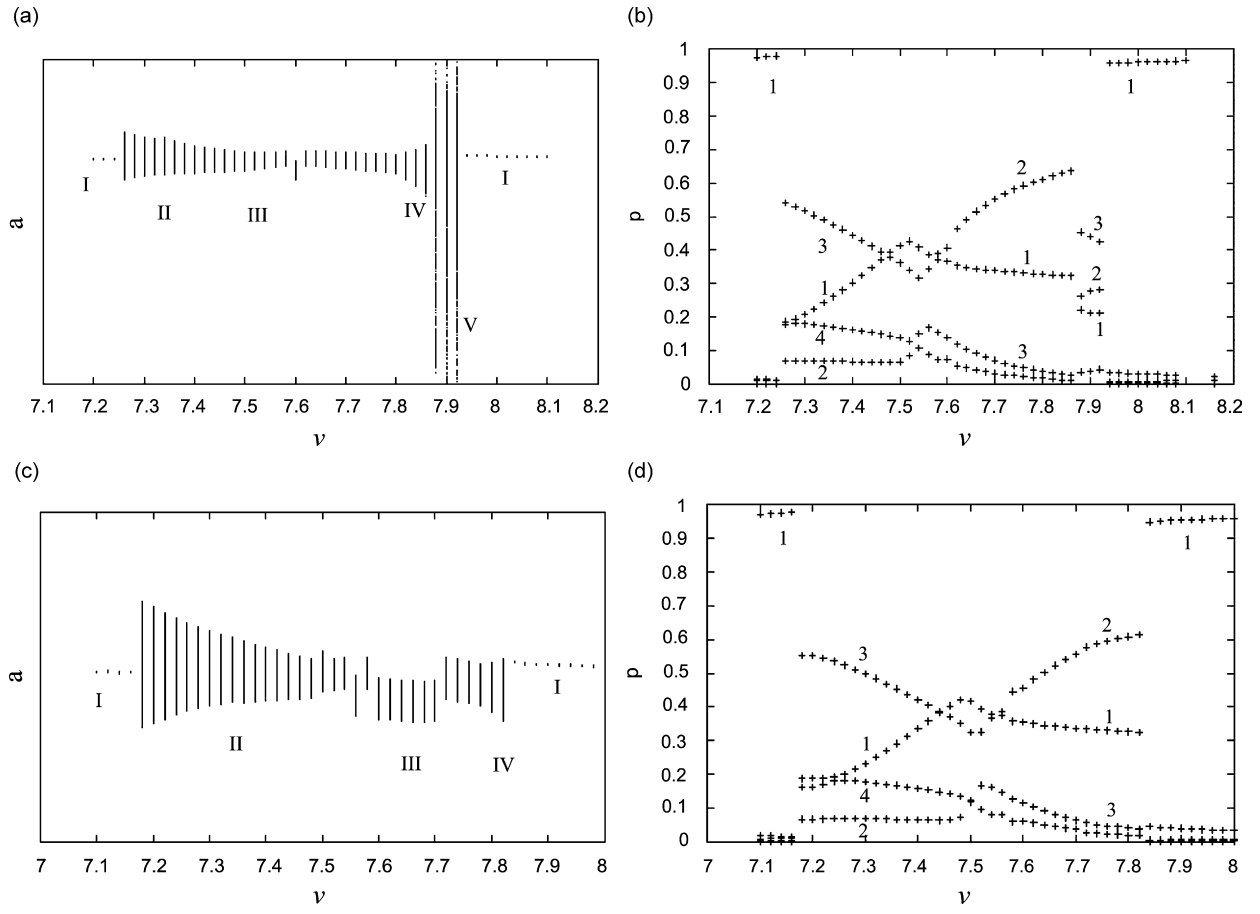

Fig. 19. Motion classes: (a), (b) for growing frequency: P1M1 (I), QP1M1$^{(+2)}$ (II), QP1M2$^{(SC,S)}$ (III), CHM2 (IV), CHM3 (V); (c), (d) for decreasing frequency: P1M1 (I), QP1M1$^{(+2)}$ (II), QP1M2$^{(SC,S)}$ (III), CHM2 (IV).

to the minimum (equal to the number of eigenvalues with zero real part at d-H bifurcation), independent of the number of mechanical d.o.f. involved in the response.

(b) Qualitative changes with respect to canonical stability diagrams possibly occur in experimental diagrams, but the d-H normal form singling out only some of the bifurcations actually organizes the overall scenario.

Characterization of CH2 response: Experimental results highlight two main ranges of nonregular response. The first one (CHM2, region E) develops on the same manifold already embedding the quasiperiodic response QP1M2$^{(S)}$ or QP1M2$^{(SC)}$. In fact, the flow decomposition does not reveal the bifurcation from quasiperiodicity to chaos neither qualitatively (no new spatial shapes are involved besides those resembling the first two in-plane and out-of-plane anti-symmetric) nor quantitatively (the singular values remain unchanged). In contrast, the second nonregular response (CHM3, region F) is characterized by the involvement of a third shape resembling the first out-of-plane symmetric mode (Figs. 19a and b and 21).

Results of a delay embedding reconstruction [25] of phase space from a time series singled out from CHM2 motion are reported in Fig. 22. Three-dimensional projections of the second order Poincaré section of the reconstructed attractor show a typical homoclinic evolution: the dynamics is organized by an unstable fixed point on the map characterized by a two-dimensional focus-stable manifold W^s and a one-dimensional saddle-unstable manifold W^u, and an invariant of the flow responsible for re-injection toward the fixed point. The fixed point on the second order Poincaré section corresponds to an unstable two-dimensional invariant of the flow resembling the formerly stable QP1M2$^{(SC)}$. In Fig. 23, besides the time series (a), two of

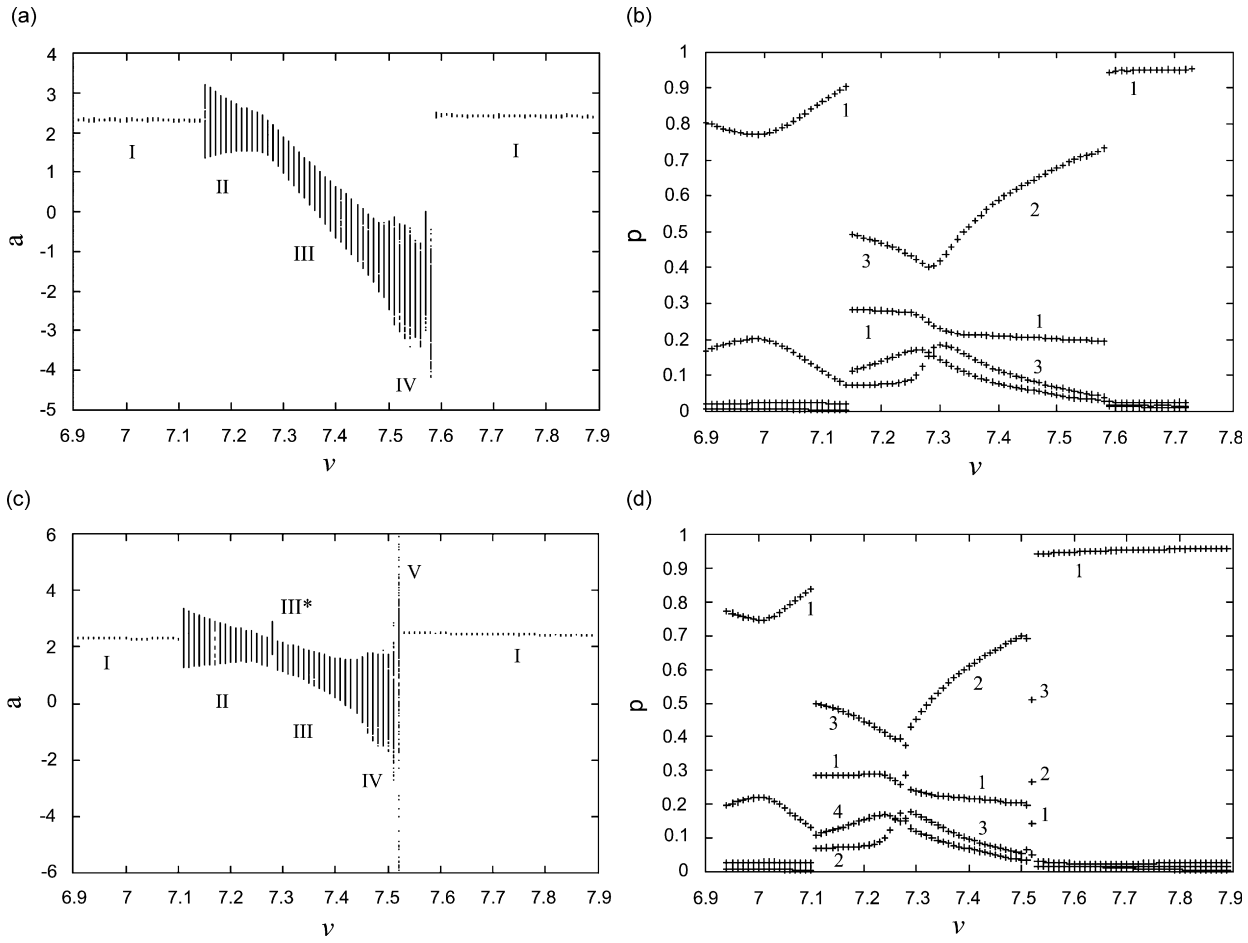

Fig. 20. Forcing amplitude (a), (b) lower than f_2, (c), (d) higher than f_2: QP1M1 (II), QP1M2$^{(SC,S)}$ (III, III*), CHM2 (IV).

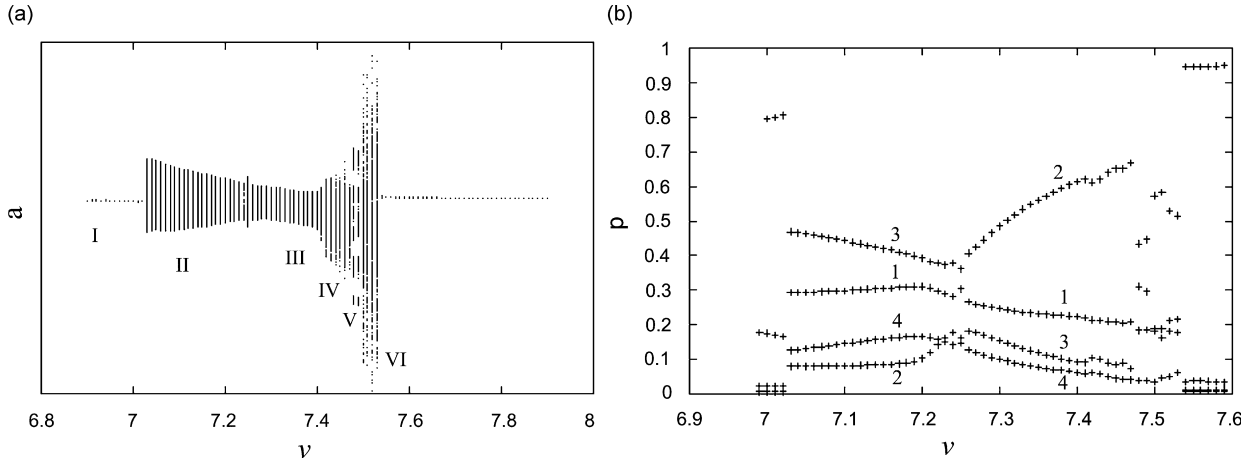

Fig. 21. Even higher forcing amplitude: CHM2 (IV), QP5M2 (V), CHM3 (VI).

the recorded homoclinic orbits are reported (b and c), showing the ejection along the two opposite directions of the unstable manifold (w direction), and the re-injection onto the stable manifold (the uv plane), respectively.

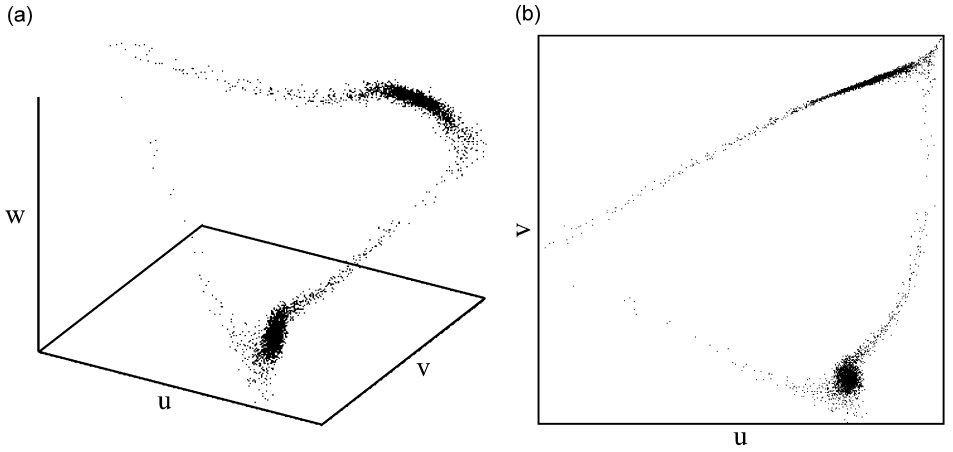

Fig. 22. Second order Poincaré map of reconstructed attractor: (a) time delay 3D reconstruction and (b) 2D projection.

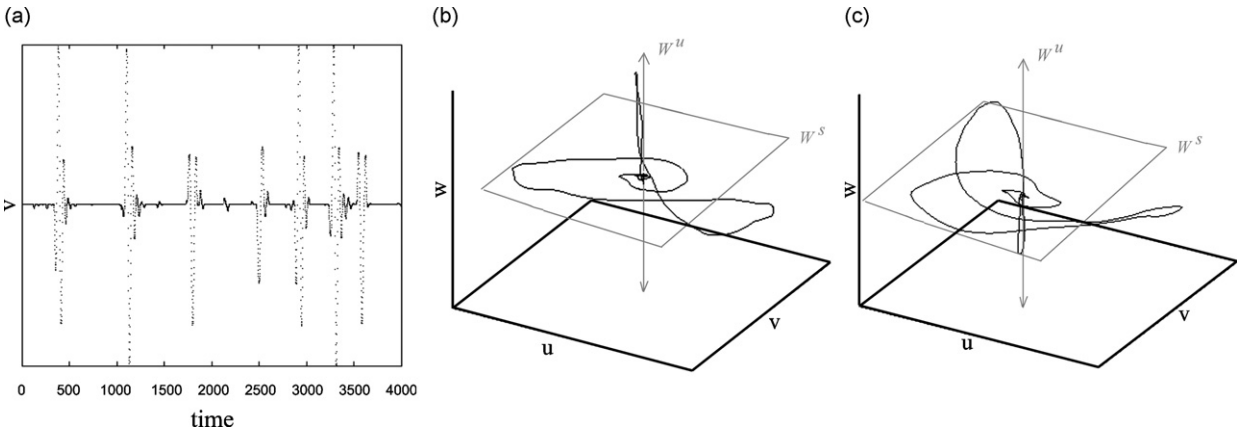

Fig. 23. Time delay reconstruction: (a) time series, (b) and (c) homoclinic orbits due to homoclinic tangency.

6.2. Chamber temperatures 2 and 0.5 °C

Results confirm the robustness of transition scenario to CHM2 (low excitation region E_1) already evidenced for higher temperatures at higher forcing amplitudes (Fig. 24).

However, the transition to CHM2 also follows an alternative path for forcing levels (f_2) sufficiently high (Fig. 25c and d), where the global bifurcation responsible of CHM2 (label V) directly affects the P5M2$^{(S)}$ (IV) due to phase locking (pl) of response QP1M2$^{(S)}$ (label III), without passing through the intermediate QP1M2$^{(SC)}$, as it commonly occurs for lower forcing amplitudes (Fig. 25a and b) or for higher temperatures. This bifurcation path to chaos is still traceable to the unfolding of the dynamics in the canonical d-H scenario (see Section 7), though being somehow richer.

Even new motion classes—already noticed at higher temperature for very high excitation amplitudes—enter the scenario: a phase locking phenomenon produces a periodic P5M2$^{(S,SC)}$ response characterized by an attractor laying on the torus already spanned by QP1M2$^{(S,SC)}$. Besides the P5M2$^{(S)}$ motion eventually evolving toward a QP5M2$^{(S)}$ response, a new nonregular region (E_3 in the behaviour chart) appears. In contrast, CHM3 region does not exist any more.

(a)

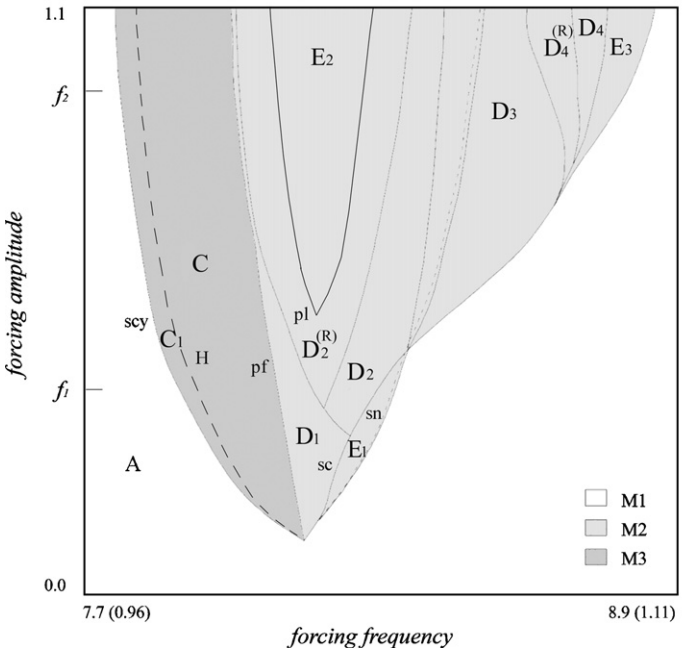

(b)

Zone		Attractor	Dimension Dc	D-T	POMs	Modes
A		P1M1	1	1	1	V_2
C		QP1M1$^{(+2)}$	2	2	1(+2)	$V_2(H_1\,V_1)$
C_1		P1M1	1	1	1	V_2
	←	QP1M1$^{(+2)}$	2	2	1(+2)	$V_2(H_1\,V_1)$
D_1	(a)	QP1M2$^{(SC),(S)}$	2	2	2	V_2H_2
	(b)	P5M2$^{(SC),(S)}$	1	2^R	2	V_2H_2
D_2		QP1M2$^{(SC),(S)}$	2	2	2	V_2H_2
$D_2^{(R)}$		P5M2$^{(SC),(S)}$	1	2^R	2	V_2H_2
D_3		QP1M2$^{(SC),(S)}$	2	2	2	V_2H_2
	←	P1M1	1	1	1	V_2
D_4		QP5M2$^{(S)}$	2	2	2	V_2H_2
	←	P1M1	1	1	1	V_2
$D_4^{(R)}$		P5M2$^{(S)(*)}$	1	2^R	2	V_2H_2
	←	P1M1	1	1	1	V_2
E_1		CHM2$^{(\#)}$	2.1		2	V_2H_2
E_2	(c)	CHM2$^{(+)}$	2.4		2	V_2H_2
	(d)	P5M2$^{(SC)}$	1	2^R	2	V_2H_2
E_3		CHM2$^{(\circ)}$	2.1		2	V_2H_2

$^{(*)}$, $^{(+)}$, $^{(\circ)}$, $^{(\#)}$ bifurcates from QP1M2$^{(S)}$, P5M2$^{(S)}$, QP5M2$^{(S)}$, QP1M2$^{(SC)}$, respectively

Fig. 24. $T = 2\,^{\circ}$C: (a) qualitative behaviour chart and (b) characterization of motion classes.

The following overall transition scheme occurs with increasing frequency:

$$\text{P1M1} \rightarrow \text{QP1M1} \rightarrow \text{QP1M2}^{(S)} \rightarrow \text{P5M2}^{(S)} \rightarrow \text{CHM2}^{(+)} \rightarrow \text{QP1M2}^{(S)} \rightarrow$$
$$\text{P5M2}^{(S)} \rightarrow \text{QP5M2}^{(S)} \rightarrow \text{CHM2}^{(\circ)} \rightarrow \text{P1M1}$$

which shows alternation of bands of quasiperiodic, phase locked regular, and nonregular responses on a manifold dominated by the two anti-symmetric shapes (POMs 1 and 2). Moreover, the ranges wherein the solutions coexist and compete with each other are wide.

Lowering the temperature to 0.5 °C provides increasing evidence of the band-like alternating structure of quasiperiodic and high-periodicity phase-locked responses. In contrast, no more chaotic response is seen to occur within the scanned parameter range, with the chosen resolution.

7. Schematic unfolding of nonregular dynamics upon divergence-Hopf bifurcation

Nonregular dynamics with M2 more directly traceable to the evolution from the d-H scenario develops relatively far from the codimension 2 bifurcation point but fits well with the regular dynamics unfolding. Main results obtained with decreasing low temperature above the d-H critical value can be summarized as follows:

- At medium temperature ($T = 6\,^{\circ}$C), transient (or structurally unstable) chaos CHM2 occurs.
- At lower temperature ($T = 3$–$4\,^{\circ}$C), depending on forcing amplitudes, two paths to steady (structurally stable) chaos CHM2 via *homoclinic explosion* (he) may occur:
  (i) from the symmetric couple QP1M2$^{(SC)}$ region:

$$\text{P1M1} \rightarrow \text{QP1M1} \rightarrow \text{QP1M2}^{(S)} \underset{\text{global}}{\longrightarrow} \text{QP1M2}^{(SC)} \underset{\text{global}}{\longrightarrow} \text{CHM2}^{(S,SC)} \rightarrow \text{CHM3}$$

  which occurs for forcing frequencies where P1M1 is unstable and further solutions with POM 3 are no more accessible (indeed, bringing the system at lower temperatures entails confining the contribution of

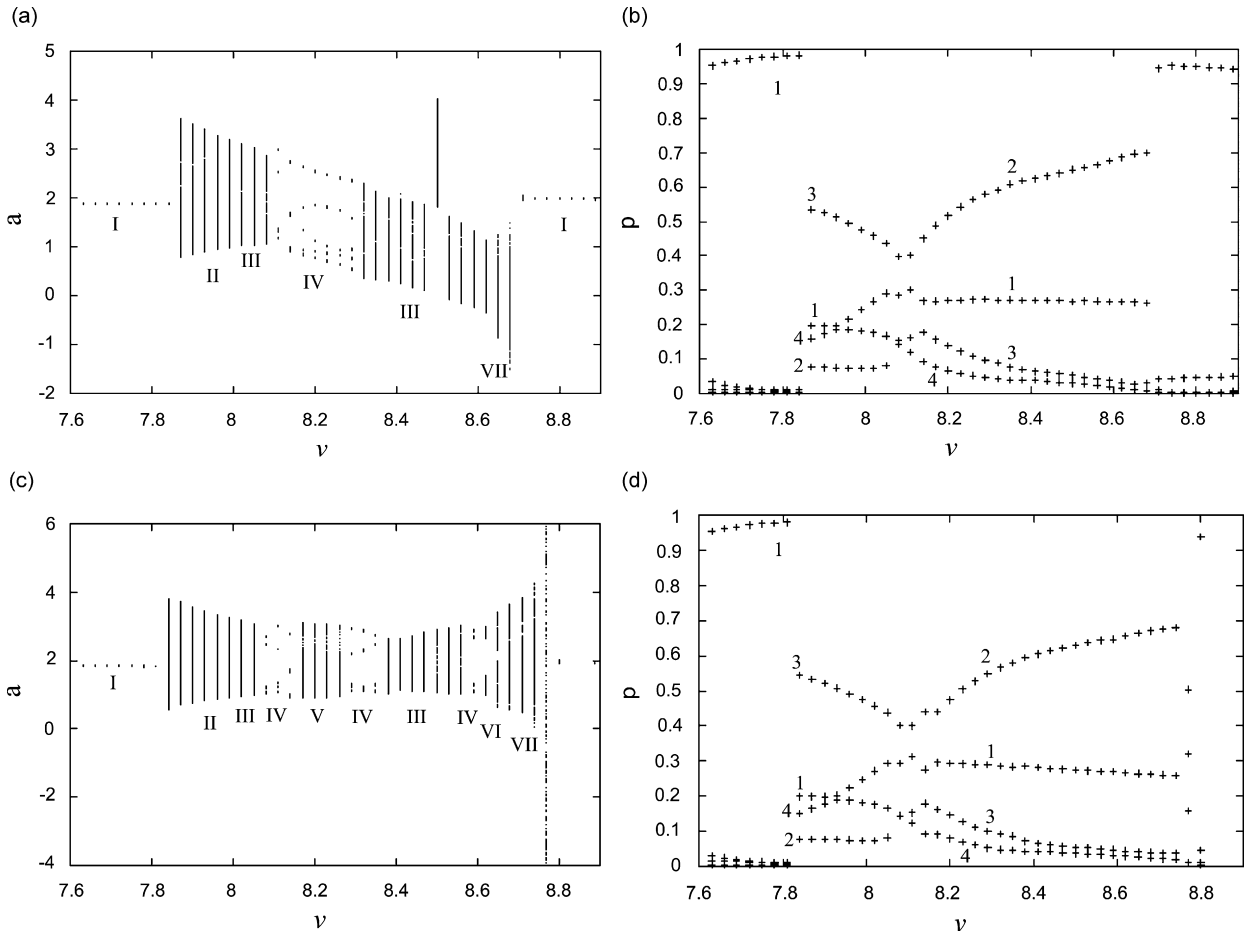

Fig. 25. Motion classes: (a, b) forcing level f_1: QP1M1 (II), QP1M2$^{(SC)}$(III), P5M2$^{(SC)}$ (IV) due to phase locking of QP1M2$^{(SC)}$, CHM2$^{(\#)}$ (VII); (c, d) forcing level f_2: besides the classes in (a, b): QP1M2$^{(S)}$ (III), new bands of chaotic CHM2$^{(+)}$ (V) and CHM2$^{(\circ)}$ (VII), periodic P5M2$^{(S)}$ (IV) and quasiperiodic QP5M2$^{(S)}$ (VI) responses are evidenced.

POM 3 to lower frequencies, thus allowing to highlight nonregular response on M2), as well as for lower forcing amplitudes;

(ii) directly from symmetric response region:

$$\mathrm{P1M1} \rightarrow \mathrm{QP1M1} \rightarrow \mathrm{QP1M2^{(S)}} \rightarrow \begin{matrix}\mathrm{P5M2^{(S)}} \\ \{\text{phase locked } \mathrm{QP1M2^{(S)}}\}\end{matrix} \underset{\text{global}}{\longrightarrow} \mathrm{CHM2^{(S,SC)}}$$

which occurs at the highest forcing amplitudes for higher temperatures, but with clear evidence also at lower forcing amplitudes for lower temperatures.

(iii) At even lower temperatures ($T<2\,^{\circ}\mathrm{C}$), further competing scenarios, dominated by phase locking phenomena, enter the response.

In any case, bifurcation diagrams for sweeping down frequency show that the stability range of P1M1 overlaps the CHM3, consistent with the hardening character of fixed point P1M1, but not the CHM2 region.

7.1. Experimental bifurcation paths (nonregular dynamics) versus theoretical stability diagram

Based on previous results, the transition to nonregular dynamics can be summarized as follows. Two homoclinic bifurcations responsible for the onset of nonregular dynamics from either symmetric (QP1M2$^{(S)}$)

or symmetric couple ($QP1M2^{(SC)}$) quasiperiodic response may occur. Homoclinic explosions originate a strange invariant set that becomes an attractor in a range of control parameters (within the instability range of P1M1), and then suddenly disappears.

It is conjectured (see the schematic stability diagram and bifurcation paths in Fig. 26) that, far away from d-H point in the stability diagram (Fig. 26a), the saddle connection locus reaches a *new codimension 2 bifurcation point* (G) where it splits into an *homoclinic explosion/implosion pair*, with an interval of stable nonregular dynamics in between. To make the experimental bifurcation scenario consistent with an interpretative theoretical scheme [31], other bifurcation branches have to emanate from G. In such a case (compare with also the bifurcation paths in Fig. 26b):

Moving anticlockwise around G:

(i) a period doubling (pd) bifurcation on (SC)-cycle (which becomes unstable) produces an unstable (S)-cycle branch reaching an homoclinic explosion where a strange invariant set is produced [32], another he (herein playing an implosion role) then destroying all unstable orbits;
(ii) the new born unstable (S)-cycle gains stability due to a sn bifurcation and emerges on the opposite side of the chaotic region.

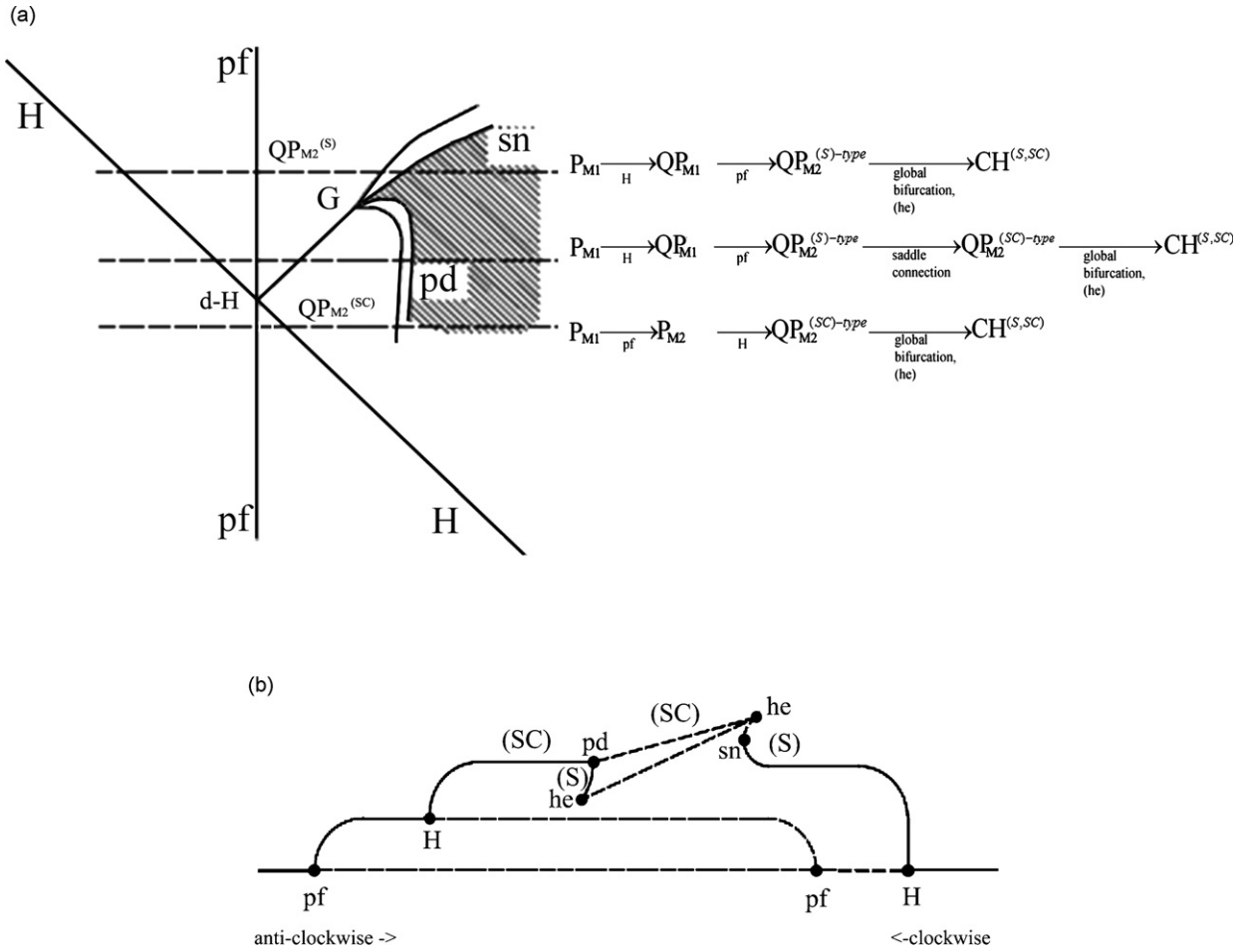

Fig. 26. Schematic (a) stability diagram and (b) experimental bifurcation paths.

Moving clockwise around G:

(i) a sn bifurcation on (S)-cycle (which becomes unstable) produces an unstable (SC)-cycle branch reaching an homoclinic explosion where a strange invariant set is produced, another he then destroying all unstable orbits;
(ii) the new born unstable (SC)-cycle gains stability due to a pd bifurcation and emerges on the opposite side of the chaotic region.

Overall, the system nonregular dynamics is consistent with the theoretical unfolding scenario ensuing from the normal form divergence-Hopf bifurcation. Yet, above the d-H point the experimental scenario is further enriched by phase-locking phenomena.

8. Conclusions and ongoing developments

Systematic experimental investigation of finite amplitude response of a multiple internally resonant suspended cable-mass, subjected to anti-phase support motion at primary resonance, has been accomplished in a parameter region wherein isolated results showed the possible occurrence of homoclinic chaos. Upon getting hints from a reference setup about the multiple bifurcation event possibly governing transition to complex dynamics, an improved experimental apparatus has been used to make the conjectured divergence-Hopf bifurcation technically accessible, while at the same time stabilizing the system and getting robust experimental outcomes. Results obtained by varying three control parameters, namely the frequency and amplitude of excitation as well as the temperature of a thermostatic chamber embedding the experimental system, have allowed us: (i) to characterize in-depth the various classes of motion in terms of time and spatial complexity, (ii) to describe peculiar and/or persistent features of transition to nonregular dynamics, and (iii) to trace them back to a canonical scenario from bifurcation theory.

As a matter of fact, improvement of the experimental analysis has been obtained also against the background of general dynamical systems knowledge, as specifically ensuing from a parallel theoretical analysis [28,29]. Availability of a third control parameter, the temperature, has shown to be fundamental for: (i) indirectly setting cable material properties to values for which, consistent with theoretical expectations, the conjectured codimension 2 bifurcation scenario to chaos has become apparent and (ii) unfolding the system dynamics not only in the strict neighbourhood of the organizing d-H bifurcation but also in the ensuing postcritical regions where the dependence of material damping on temperature affects secondary bifurcations to homoclinic chaos.

In general terms, varying the temperature of the thermally conditioned system has allowed the authors:

- to distinguish between otherwise undistinguishable critical thresholds (surfaces in 3D control space) and recognize an underlying *common invariant bifurcation structure*, otherwise hidden by the inherent complexity of the infinite-dimensional system dynamics;
- to refer qualitatively the *experimental unfolding* of *regular* and *nonregular* cable dynamics in the considered frequency range to the *theoretical* unfolding of the divergence-Hopf bifurcation normal form;
- to characterize the occurrence and robustness of response transition to *low-dimensional* (two POMs, i.e., mechanical variables) *homoclinic chaos*;
- to show the *variable involvement*, in either quasiperiodic or chaotic responses, of a *further* POM with respect to the reference normal form scenario.

Specifically, temperature variations have been seen to affect: (i) the locus of codimension 2 bifurcation point in the frequency-amplitude behaviour chart, whose critical forcing value decreases with decreasing temperature, still guaranteeing cable tension; (ii) the system dimensionality in the neighbourhood of the critical point, wherein a further POM resembling the first symmetric out-of-plane mode is driven in the response besides the dominating in-plane and out-of-plane antisymmetric POMs; (iii) the variable details of the post-critical evolution with varying forcing frequency, within the dominant scenario; and (iv) the robustness of the latter, which is replaced by other scenarios at the lowest temperatures.

Parallel ongoing theoretical studies [29] are concerned with developing a consistent phenomenologically based two-d.o.f. model of the suspended cable. Availability of such a reduced order model and its analytical-numerical solution will allow us to check: (i) the pursued theoretical interpretation of the dominant experimental scenario along with the possibility to (partially) reproduce it and (ii) the likely need to account for also the resonant contribution of a third d.o.f. for actually reproducing the richness of experimental results in the post-critical range.

References

[1] G. Rega, Nonlinear dynamics of suspended cables. Part I: modeling and analysis; part II: deterministic phenomena, *ASME Applied Mechanics Reviews* 57 (2004) 443–514.
[2] R.A. Ibrahim, Nonlinear vibrations of suspended cables. Part III: random excitation and interaction with fluid flow, *ASME Applied Mechanics Reviews* 57 (2004) 515–549.
[3] N. Srinil, G. Rega, S. Chucheepsakul, Two-to-one resonant multi-modal dynamics of horizontal/inclined cables. Part I: theoretical formulation and model validation, *Nonlinear Dynamics* 48 (2007) 231–252.
[4] N. Srinil, G. Rega, Two-to-one resonant multi-modal dynamics of horizontal/inclined cables. Part II: internal resonance activation, reduced order models and nonlinear normal modes, *Nonlinear Dynamics* 48 (2007) 253–274.
[5] N.C. Perkins, Modal interactions in the non-linear response of elastic cables under parametric/external excitation, *International Journal of Non-linear Mechanics* 27 (1992) 233–250.
[6] C.L. Lee, N.C. Perkins, Experimental investigation of isolated and simultaneous internal resonances in suspended cables, in: R.A. Ibrahim, A.K. Bajaj, L.A. Bergman (Eds.), *Nonlinear Vibrations*, Vol. DE-54, ASME, New York, 1993, pp. 21–31.
[7] Y. Fujino, T. Susumpow, An experimental study on active control of in-plane cable vibration by axial support motion, *Earthquake Engineering & Structural Dynamics* 23 (1994) 1283–1297.
[8] Y.L. Xu, Z. Yu, Non-linear vibration of cable-damper systems. Part II: application and verification, *Journal of Sound and Vibration* 225 (1999) 465–481.
[9] A. Berlioz, C.H. Lamarque, Nonlinear vibrations of an inclined cable, *ASME Journal of Vibration and Acoustics* 127 (2005) 315–323.
[10] V. Gattulli, R. Alaggio, F. Potenza, Analytical prediction and experimental validation for longitudinal control of cable oscillations, *International Journal of Non-linear Mechanics* 43 (2008) 36–52.
[11] G. Rega, R. Alaggio, F. Benedettini, Experimental investigation of the nonlinear response of a hanging cable. Part I: local analysis, *Nonlinear Dynamics* 14 (1997) 89–117.
[12] F. Benedettini, G. Rega, Experimental investigation of the nonlinear response of a hanging cable. Part II: global analysis, *Nonlinear Dynamics* 14 (1997) 119–138.
[13] R. Alaggio, G. Rega, Characterizing bifurcations and classes of motion in the transition to chaos through 3D-tori of a continuous experimental system in solid mechanics, *Physica D* 137 (2000) 70–93.
[14] G. Rega, R. Alaggio, Spatio-temporal dimensionality in the overall complex dynamics of an experimental cable/mass system, *International Journal of Solids and Structures* 38 (2001) 2049–2068.
[15] J. Guckenheimer, P. Holmes, *Nonlinear Oscillations*, *Dynamical Systems*, *Bifurcation of Vector Fields*, Applied Mathematical Sciences, Vol. 42, Springer, New York, 1983.
[16] Y.A. Kuznetsov, *Elements of Applied Bifurcation Theory*, Applied Mathematical Sciences, Vol. 112, Springer, New York, 1998.
[17] P. Glendinning, C. Sparrow, Local and global behaviour near homoclinic orbits, *Journal of Statistical Physics* 35 (1984) 645–696.
[18] L. Shilnikov, A. Shilnikov, D. Turaev, L. Chua, *Methods of Qualitative Theory in Nonlinear Dynamics*, World Scientific Series on Nonlinear Science Series A, Vol. 4, World Scientific Publishers, Singapore, 1998.
[19] G. Dangelmayr, E. Knobloch, The Takens–Bogdanov bifurcation with O(2)-symmetry, *Philosophical Transactions of the Royal Society London A* 322 (1987) 243–279.
[20] D.H. Sattinger, *Group Theoretic Methods in Bifurcation Theory*, Lecture Notes in Mathematics, Vol. 762, Springer, Berlin, 1979.
[21] A.R. Champneys, V. Kirk, The entwined wiggling of homoclinic curves emerging from saddle-node/Hopf instabilities, *Physica D* 195 (2004) 77–105.
[22] N.H. Packard, J.P. Crutchfield, J.D. Farmer, R.S. Shaw, Geometry from a time series, *Physical Review Letters* 45 (1980) 712–716.
[23] R. Mané, *On the Dimension of the Compact Invariant Sets of Certain Nonlinear Maps*, in: *Dynamical Systems and Turbulence*, Springer, Berlin, 1981, pp. 230–242.
[24] F. Takens, *Detecting Strange Attractors in Turbulence*, in: *Dynamical Systems and Turbulence*, Springer, Berlin, 1981, pp. 366–381.
[25] T. Sauer, J.A. Yorke, M. Casdagli, Embedology, *Journal of Statistical Physics* 65 (1991) 579–616.
[26] P. Grassberger, I. Procaccia, Measuring the strangeness of strange attractors, *Physica D* 9 (1983) 189–208.
[27] P. Holmes, J.L. Lumley, G. Berkooz, *Turbulence*, *Coherent Structures*, Dynamical Systems and Symmetry, Cambridge University Press, Cambridge, 1996.

[28] G. Rega, R. Alaggio, Experimental characterization and theoretical model of a homoclinic bifurcation to chaos in a cable-mass system, *Third International Conference on Advances in Mechanical Engineering and Mechanics*, Hammamet, 2006, pp. 84–86.
[29] R. Alaggio, G. Rega, Phenomenological model of the experimental bifurcation scenario of a polymeric cable exhibiting low-dimensional homoclinic chaos, *International Conference Nonlinear Phenomena in Polymer Solids and Low-dimensional Systems*, Moscow, 2008.
[30] H. Troger, A. Steindl, *Nonlinear Stability and Bifurcation Theory*, Springer, Wien, 1991.
[31] A.M. Rucklidge, Chaos in a low-order model of magnetoconvection, *Physica D* 62 (1993) 323–337.
[32] S. Wiggins, *Global Bifurcation and Chaos*: *Analytical Methods*, Applied Mathematical Sciences, Vol. 73, Springer, New York, 1988.